Computational and Kinetics Analyses of an Aminomutase using Ring-substituted Arylalanines Reveal that Sterics and Substituent Effects Dictate Substrate Specificity

Nishanka Dilini Ratnayake,[†‡] Nan Liu,[†^‡] Leslie A. Kuhn,[^#] and Kevin D. Walker[#†*]*

[†]Department of Chemistry, [#]Department of Biochemistry and Molecular Biology, and [^]Computer Science & Engineering, Michigan State University, East Lansing, MI 48824.

Corresponding Authors

*walke284@msu.edu; kuhnl@msu.edu

Supporting Information

Contents

Substrates, Authentic Standards and Reagents

(*S*)-α-, *p*-Methoxy-(*S*)-α-, *p*-nitro-(*S*)-α-, and *p*-chloro-(*R*/*S*)-β-phenylalanine and (*E*)-*o*-methyl-, (*E*)-*p*-methyl-, (*E*)-*p*-methoxy- and (*E*)-*p*-nitro-cinnamic acid, (*E*)-*o*-furyl-acrylate and (trimethylsilyl)diazomethane (2.0 M in diethyl ether) were purchased from Sigma-Aldrich-Fluka (St. Louis, MO). Racemic *p*-nitro-β-phenylalanine was purchased from Oakwood Products, Inc. (West Columbia, SC), and *o*-methoxy-(*S*)-α-, *m*-methoxy-(*S*)-α-, *o*-nitro-(*S*)-α-, *m*-nitro-(*S*)-α-, *o*-methoxy-(*S*)-β-, *m*-methoxy-(*S*)-β-, *o*-nitro-(*S*)-β-, and *m*-nitro-(*S*)-β-phenylalanine were purchased from Chem-Impex International, Inc. (Wood Dale, IL). 2-Amino-5-phenylpentanoic acid was purchased from Acros Organics (New Jersey). All other (*S*)-α- and β-amino acids were purchased from PepTech Corporation (Burlington, MA) and the other (*E*)-cinnamic acids were purchased from Alfa Aesar (Ward, Hill, MA). All chemicals were used without further purification, unless noted.

General Instrumentation

GC-MS analysis was performed with an Agilent 6890N gas chromatograph equipped with a capillary GC column (30 m × 0.25 mm × 0.25 μM; HP-5MS; J&W Scientific) with helium as the carrier gas (flow rate, 1 mL/min). The injector port (at 250 °C) was set to splitless injection mode. A 1-μL aliquot of each sample was injected using an Agilent 7683 auto-sampler (Agilent, Atlanta; GA). The column temperature was increased from 50 – 110 °C at 30 °C/min, then increased by 10 °C/min to 250 °C (total run time of 16 min), and returned to 50 °C over 5 min, with a 5 min hold. The gas chromatograph was coupled to a mass selective detector (Agilent, 5973 *inert*) operated in electron impact mode (70 eV ionization voltage). All spectra were recorded in the mass range of 50 – 400 *m*/*z*.

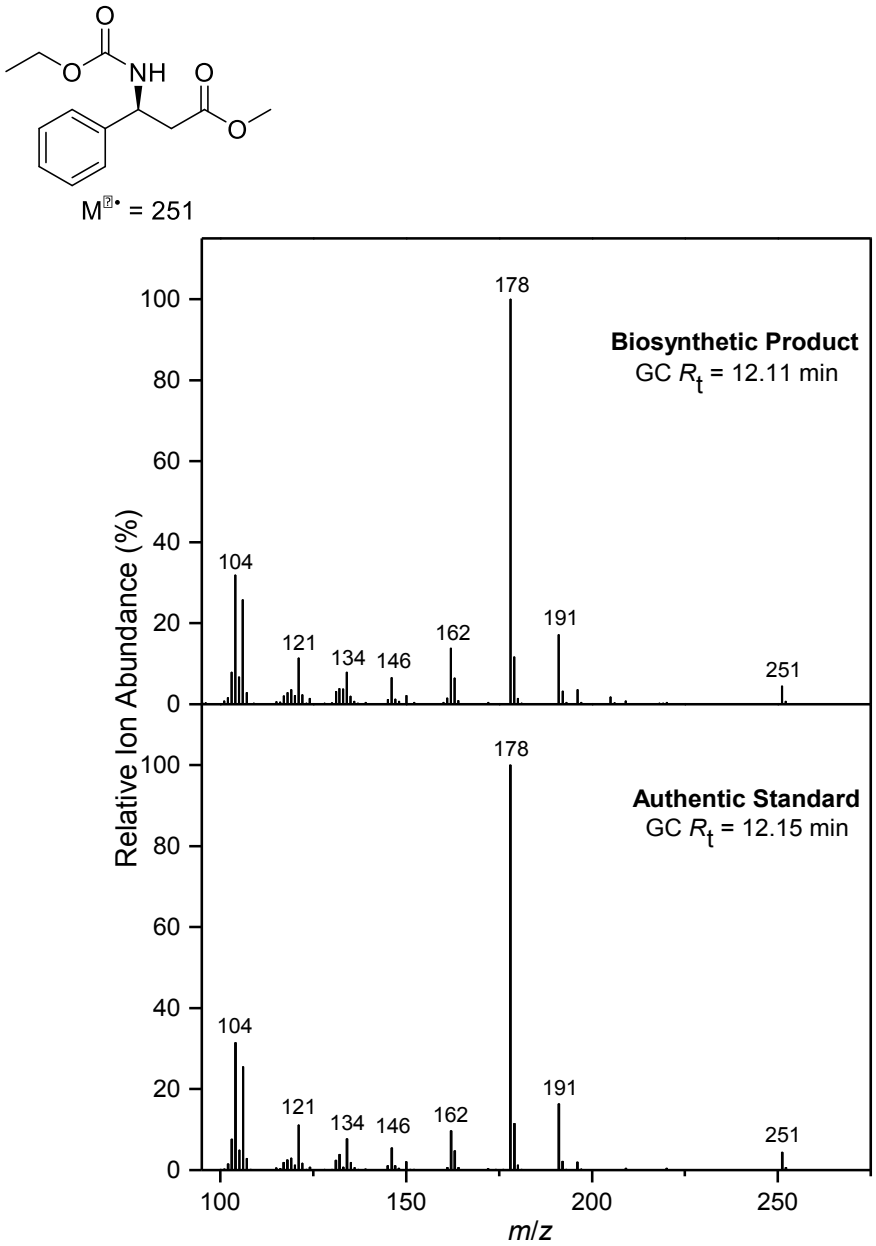

Figure S1. EI-MS spectra of the *N*-(ethoxycarbonyl) methyl ester derivatives of biosynthetic β-phenylalanine made from *Pa*PAM catalysis (top) and authentic β-phenylalanine (bottom). GC retention times (GC R_t) are shown.

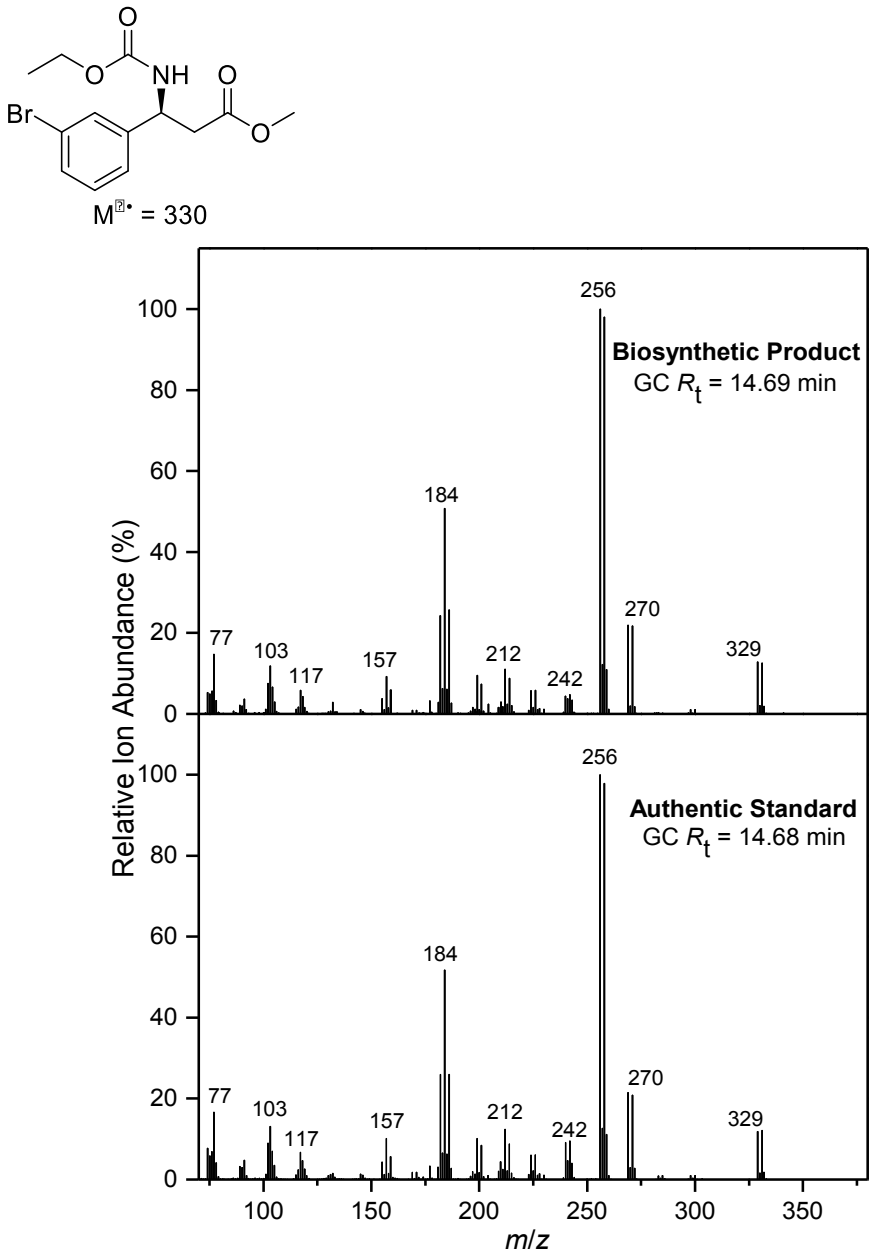

Figure S2. EI-MS spectra of the *N*-(ethoxycarbonyl) methyl ester derivatives of biosynthetic *m*-bromo-β-phenylalanine made from *Pa*PAM catalysis (top) and authentic *m*-bromo-β-phenylalanine (bottom). GC retention times (GC R_t) are shown.

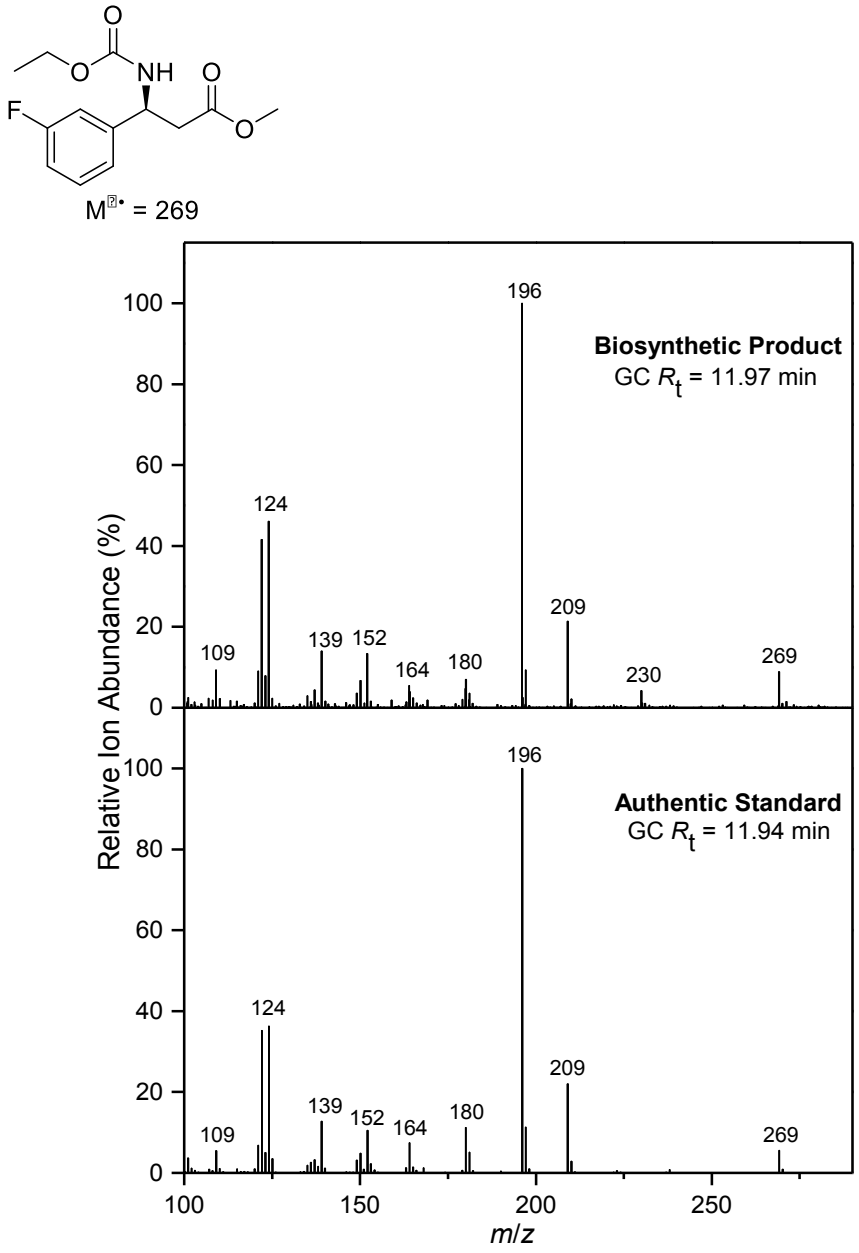

Figure S3. EI-MS spectra of the *N*-(ethoxycarbonyl) methyl ester derivatives of biosynthetic *m*-fluoro-β-phenylalanine made from *Pa*PAM catalysis (top) and authentic *m*-fluoro-β-phenylalanine (bottom). GC retention times (GC R_t) are shown.

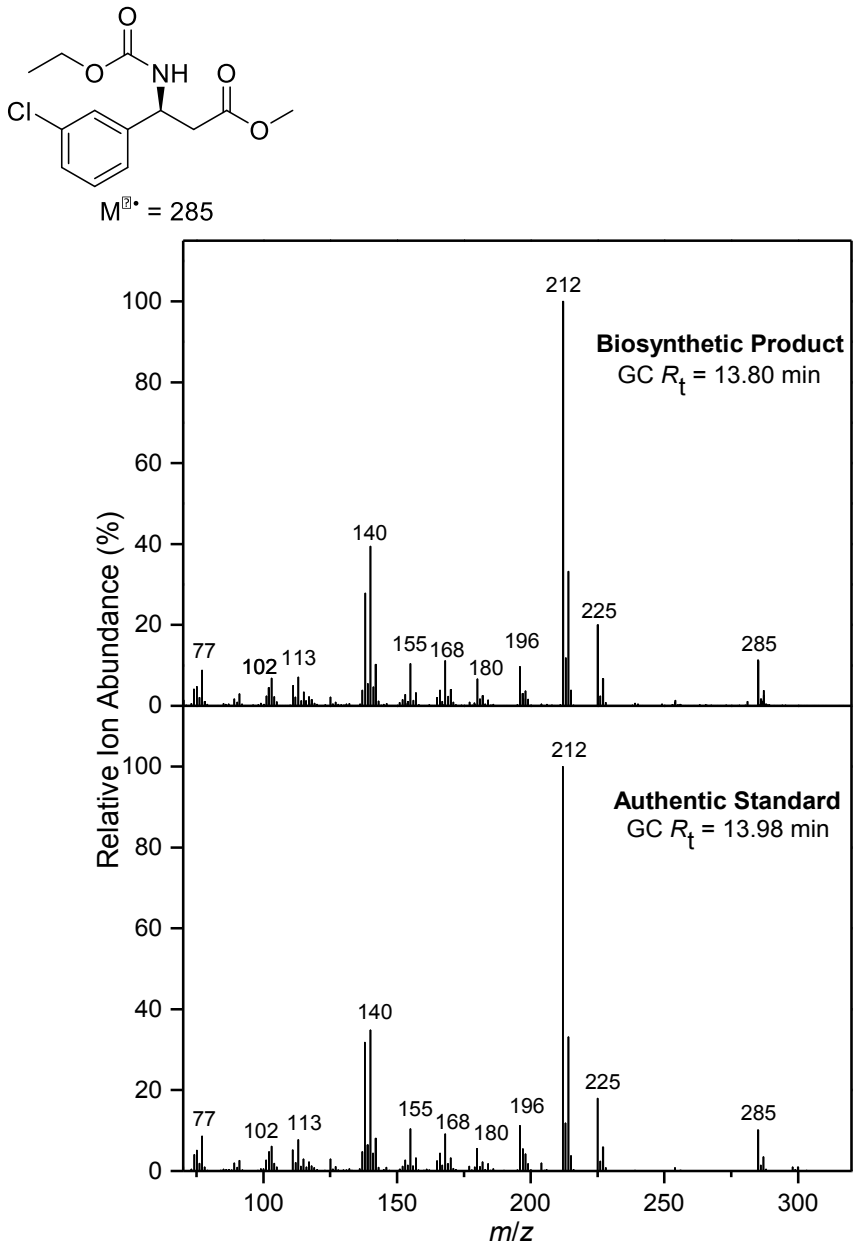

Figure S4. EI-MS spectra of the *N*-(ethoxycarbonyl) methyl ester derivatives of biosynthetic *m*-chloro-β-phenylalanine made from *Pa*PAM catalysis (top) and authentic *p*-chloro-β-phenylalanine (bottom). GC retention times (GC R_t) are shown. Note, *p*-chloro-β-phenylalanine was on-hand and used as the authentic standard.

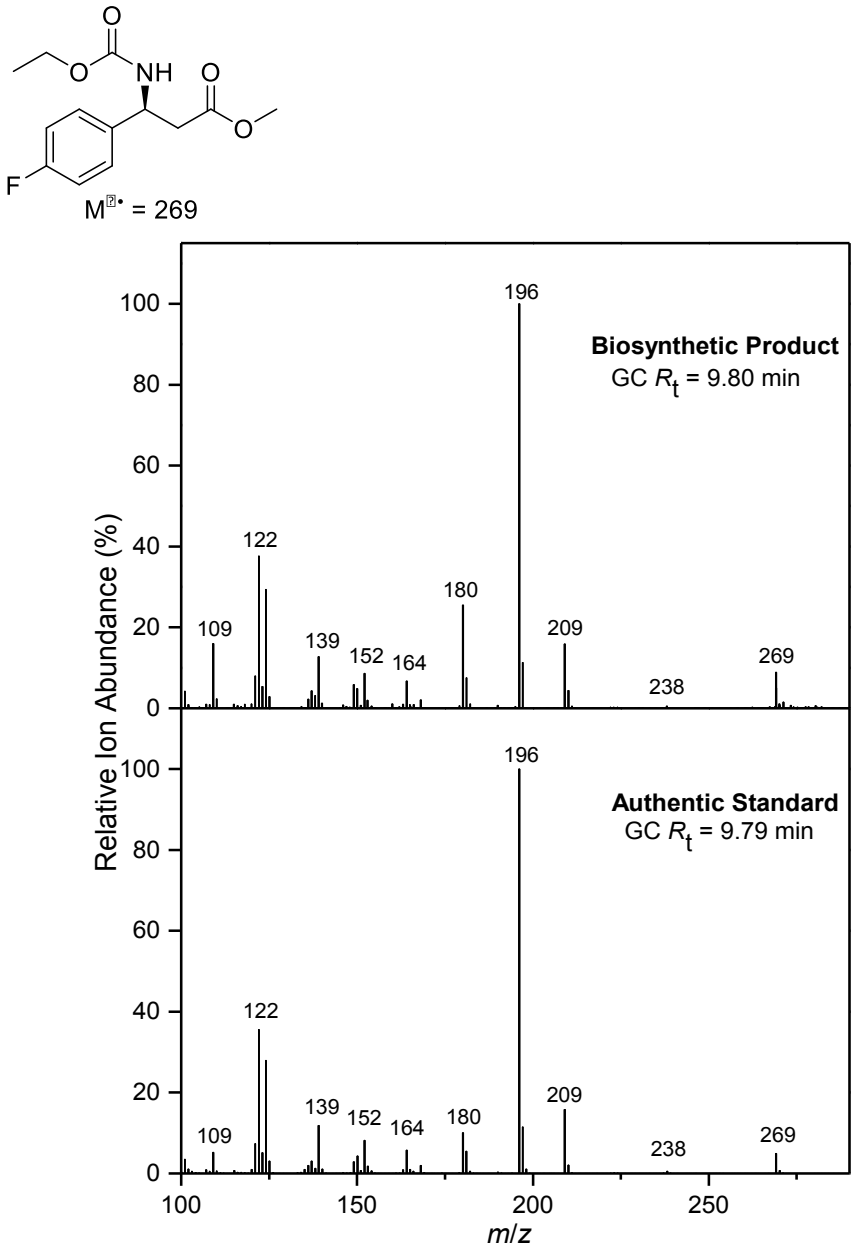

Figure S5. EI-MS spectra of the *N*-(ethoxycarbonyl) methyl ester derivatives of biosynthetic *p*-fluoro-β-phenylalanine made from *Pa*PAM catalysis (top) and authentic *p*-fluoro-β-phenylalanine (bottom). GC retention times (GC R_t) are shown.

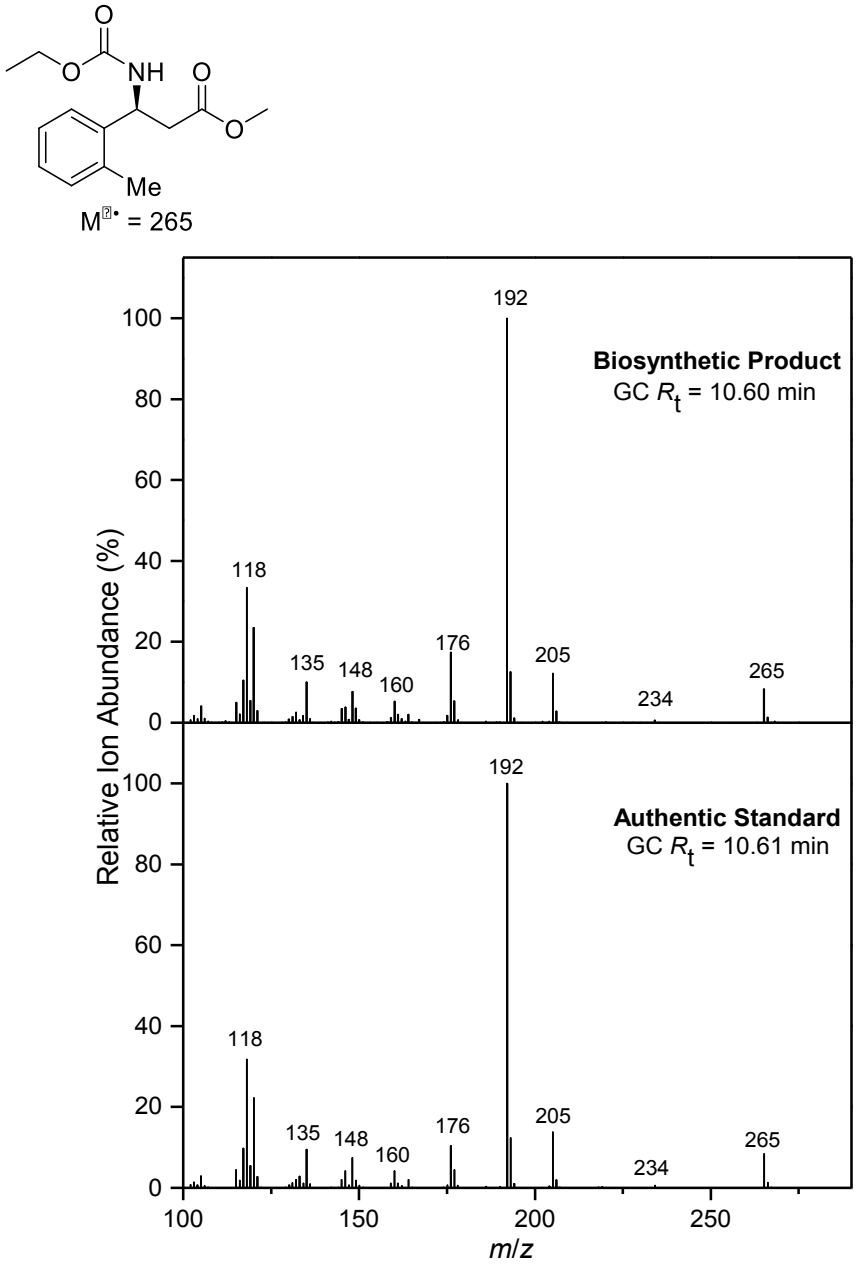

Figure S6. EI-MS spectra of the *N*-(ethoxycarbonyl) methyl ester derivatives of biosynthetic *o*-methyl-β-phenylalanine made from *Pa*PAM catalysis (top) and authentic *o*-methyl-β-phenylalanine (bottom). GC retention times (GC R_t) are shown.

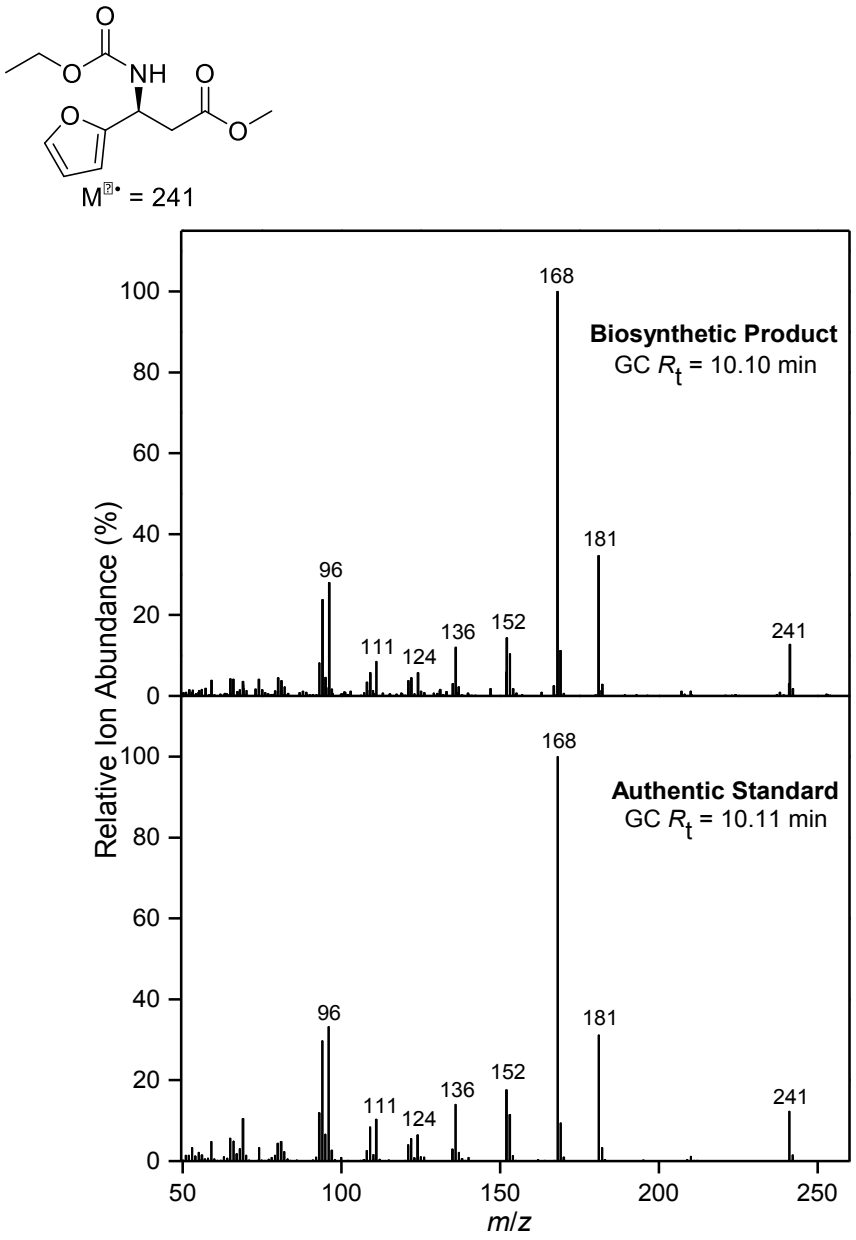

Figure S7. EI-MS spectra of the *N*-(ethoxycarbonyl) methyl ester derivatives of biosynthetic 2-furyl-β-alanine made from *Pa*PAM catalysis (top) and authentic 2-furyl-β-alanine (bottom). GC retention times (GC R_t) are shown.

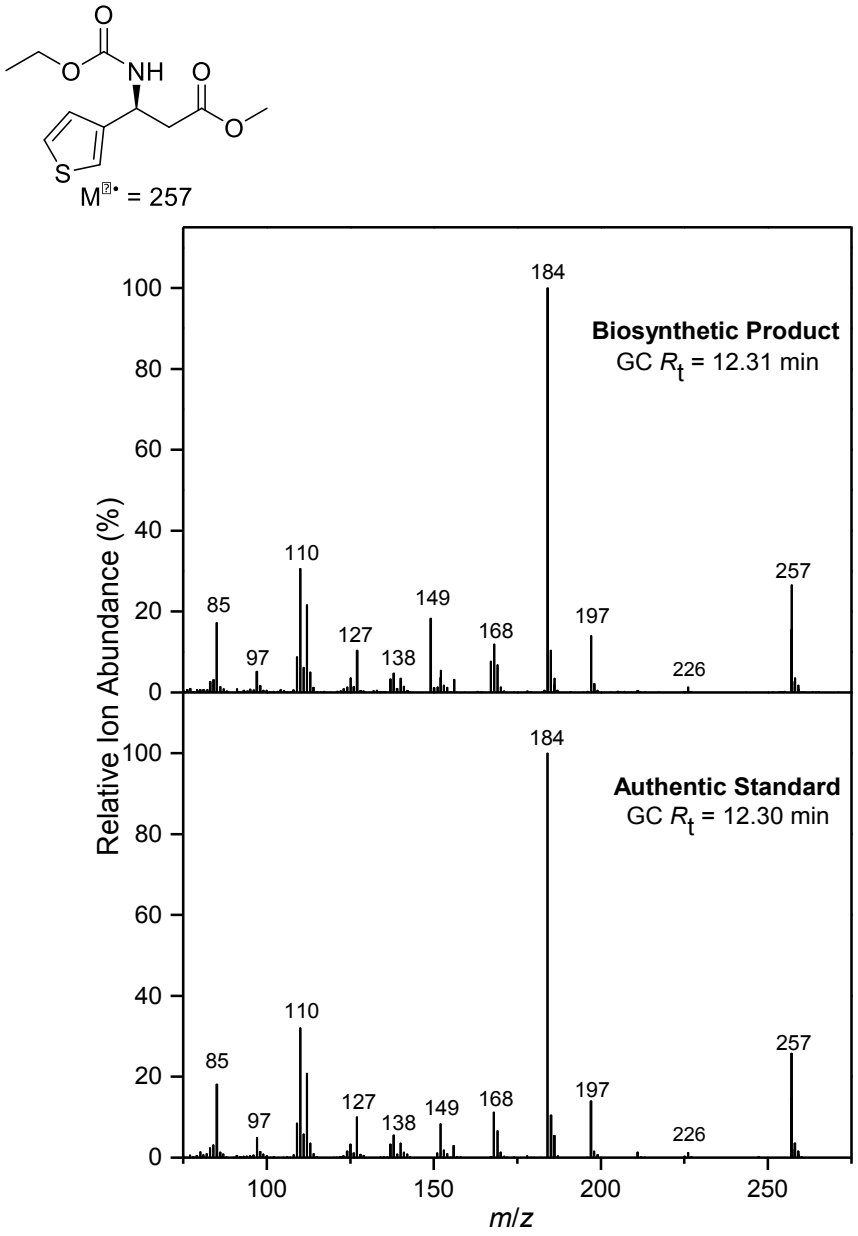

Figure S8. EI-MS spectra of the *N*-(ethoxycarbonyl) methyl ester derivatives of biosynthetic 3-thienyl-β-alanine made from *Pa*PAM catalysis (top) and authentic 3-thienyl-β-alanine (bottom). GC retention times (GC R_t) are shown.

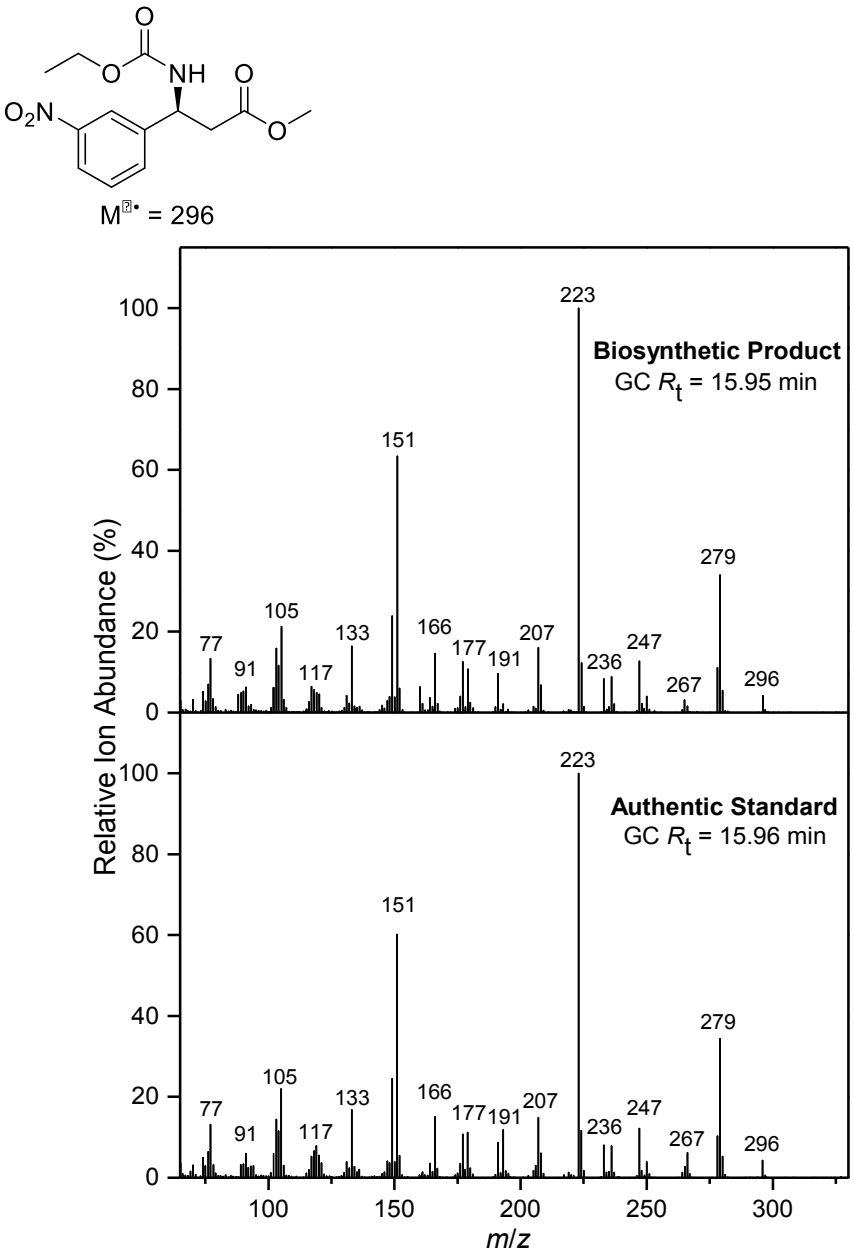

Figure S9. EI-MS spectra of the *N*-(ethoxycarbonyl) methyl ester derivatives of biosynthetic *m*-nitro-β-phenylalanine made from *Pa*PAM catalysis (top) and authentic *m*-nitro-β-phenylalanine (bottom). GC retention times (GC R_t) are shown.

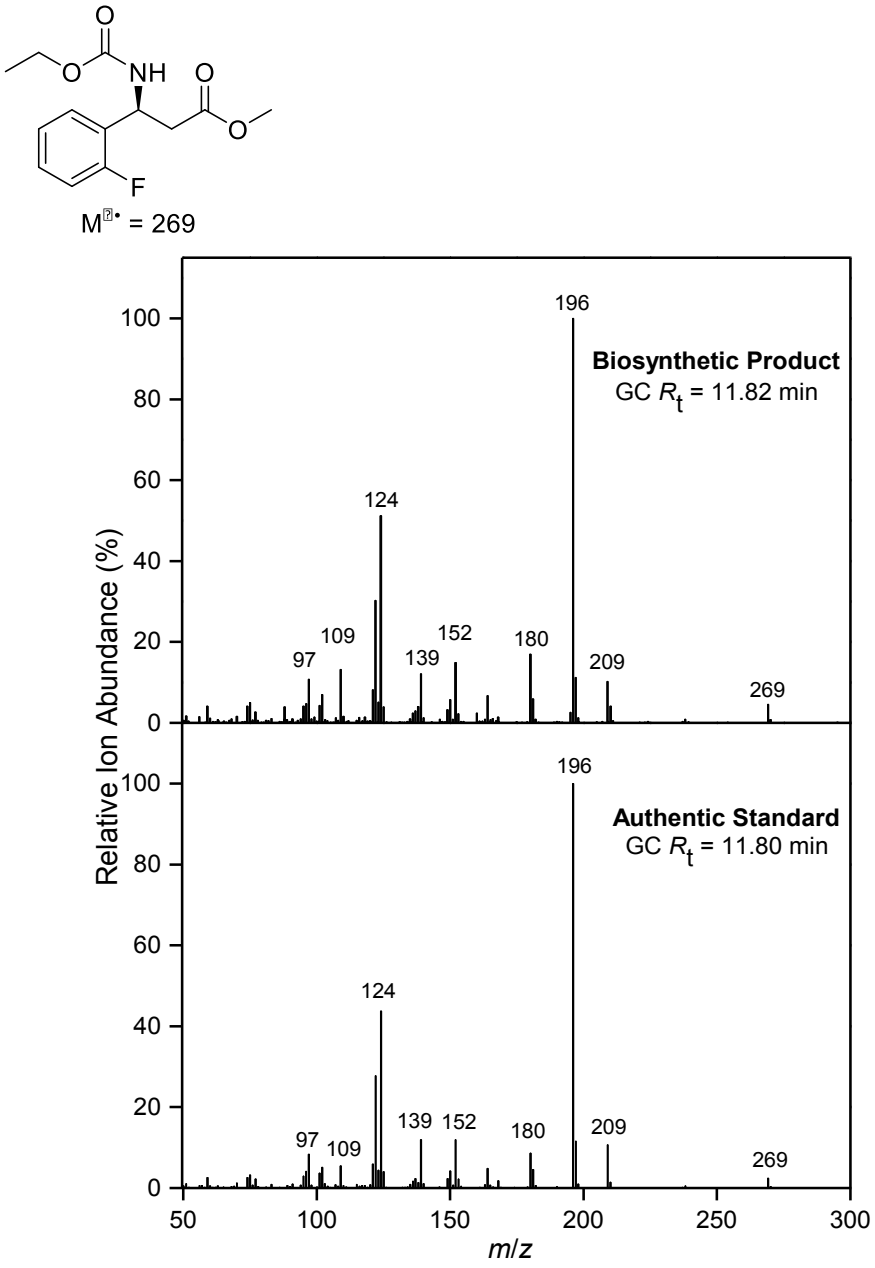

Figure S10. EI-MS spectra of the *N*-(ethoxycarbonyl) methyl ester derivatives of biosynthetic *o*-fluoro-β-phenylalanine made from *Pa*PAM catalysis (top) and authentic *o*-fluoro-β-phenylalanine (bottom). GC retention times (GC R_t) are shown.

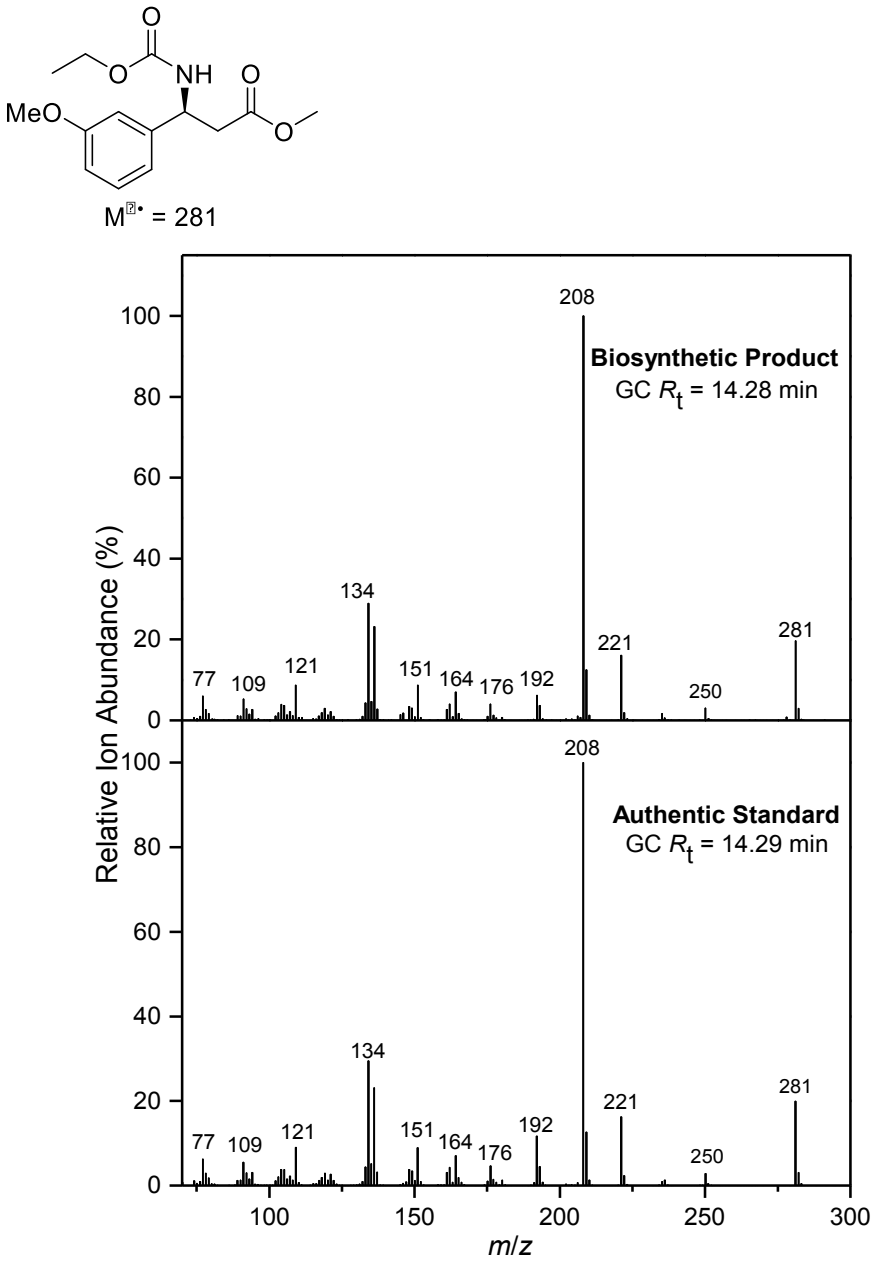

Figure S11. EI-MS spectra of the *N*-(ethoxycarbonyl) methyl ester derivatives of biosynthetic *m*-methoxy-β-phenylalanine made from *Pa*PAM catalysis (top) and authentic *m*-methoxy-β-phenylalanine (bottom). GC retention times (GC R_t) are shown.

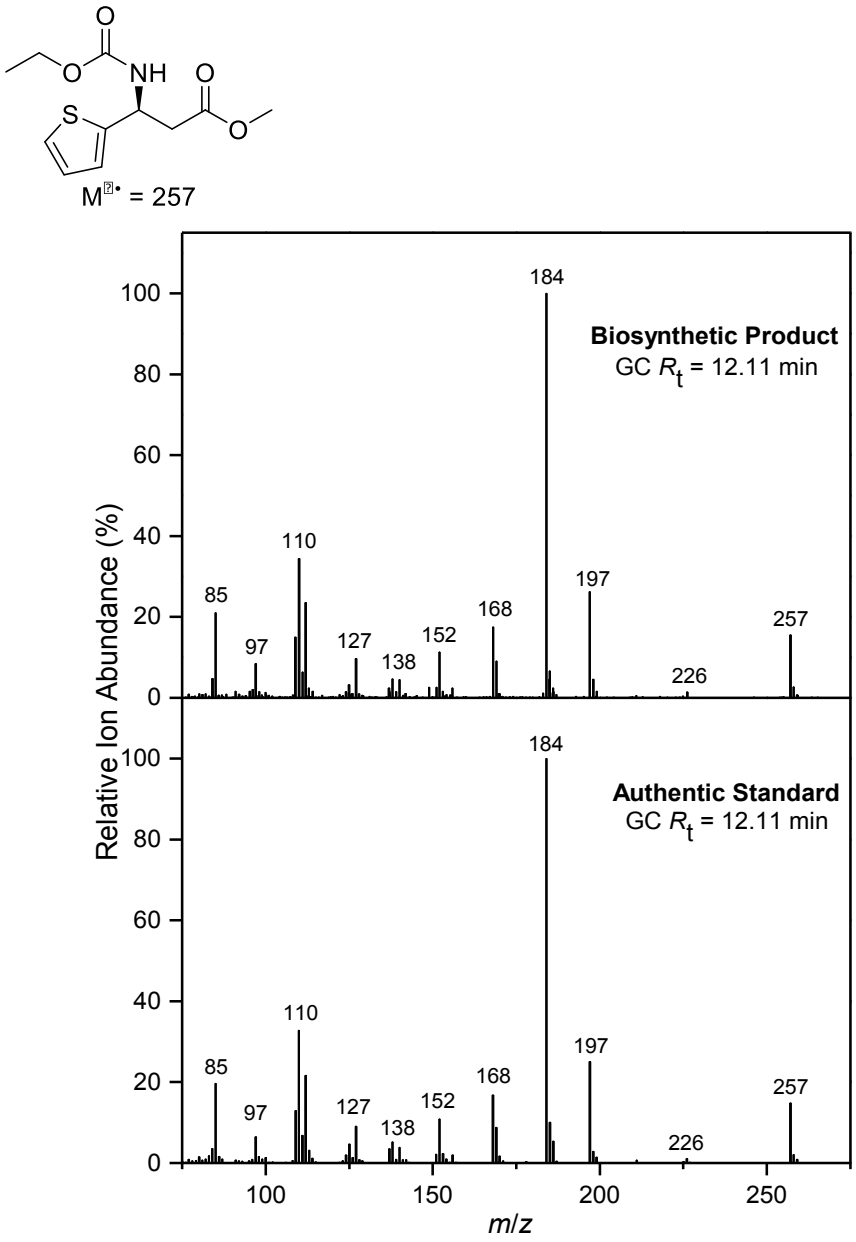

Figure S12. EI-MS spectra of the *N*-(ethoxycarbonyl) methyl ester derivatives of biosynthetic 2-thienyl-β-alanine made from *Pa*PAM catalysis (top) and authentic 2-thienyl-β-alanine (bottom). GC retention times (GC R_t) are shown.

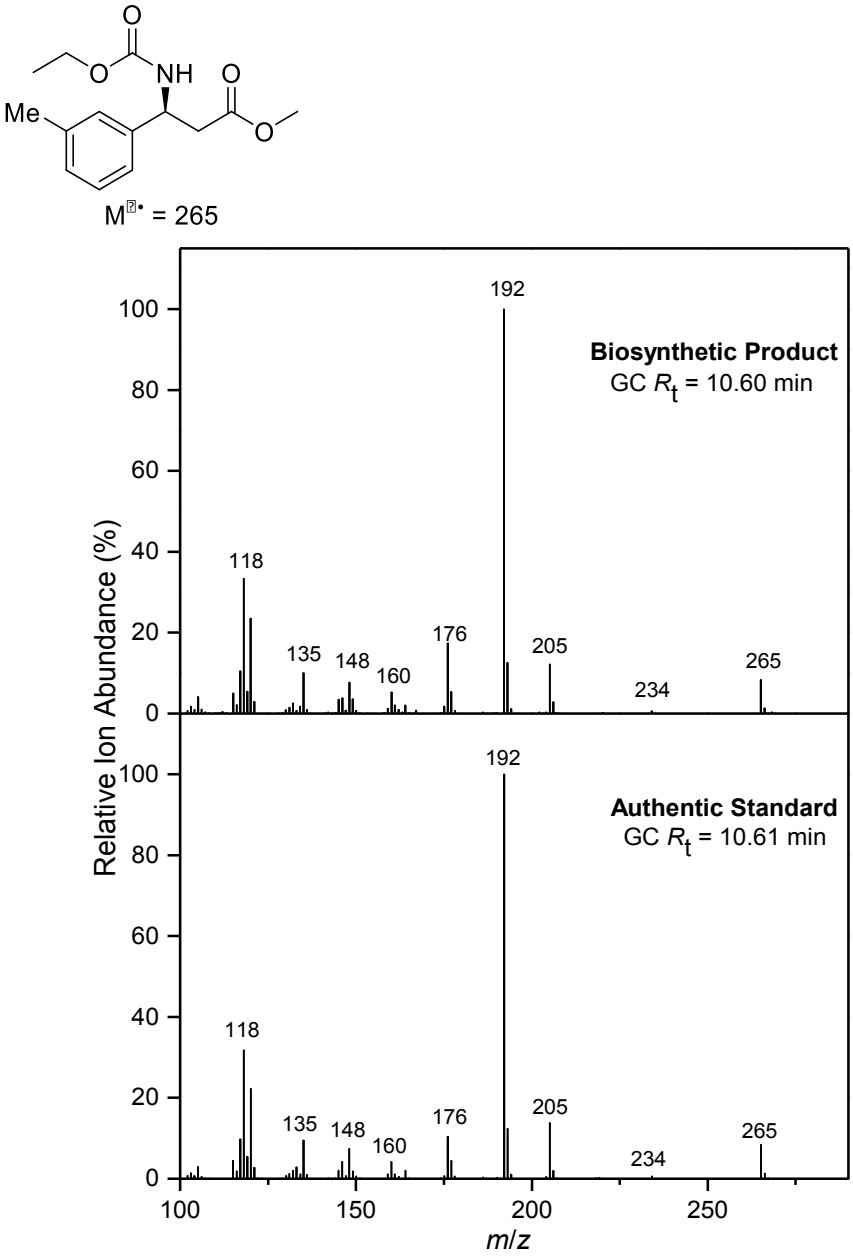

Figure S13. EI-MS spectra of the *N*-(ethoxycarbonyl) methyl ester derivatives of biosynthetic *m*-methyl-β-phenylalanine made from *Pa*PAM catalysis (top) and authentic *m*-methyl-β-phenylalanine (bottom). GC retention times (GC R_t) are shown.

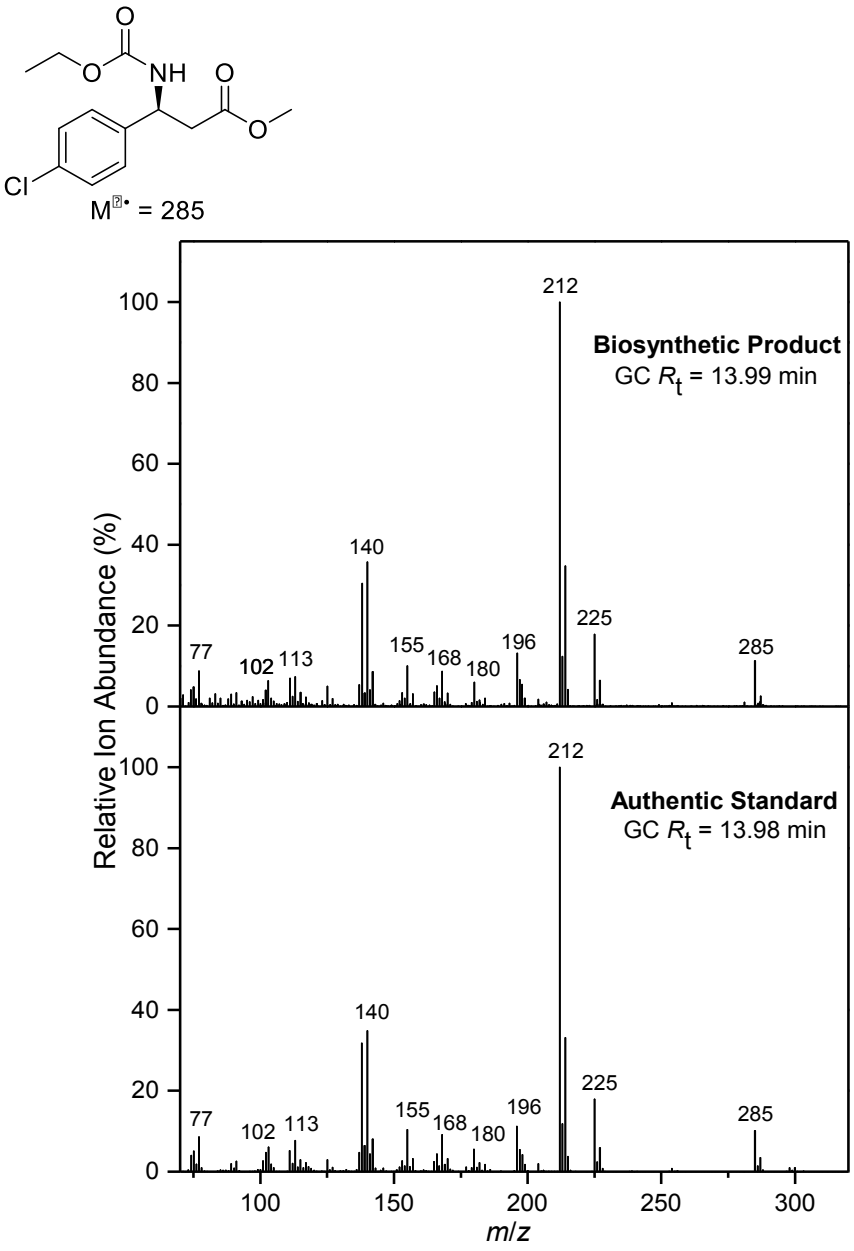

Figure S14. EI-MS spectra of the *N*-(ethoxycarbonyl) methyl ester derivatives of biosynthetic *p*-chloro-β-phenylalanine made from *Pa*PAM catalysis (top) and authentic *p*-chloro-β-phenylalanine (bottom). GC retention times (GC R_t) are shown.

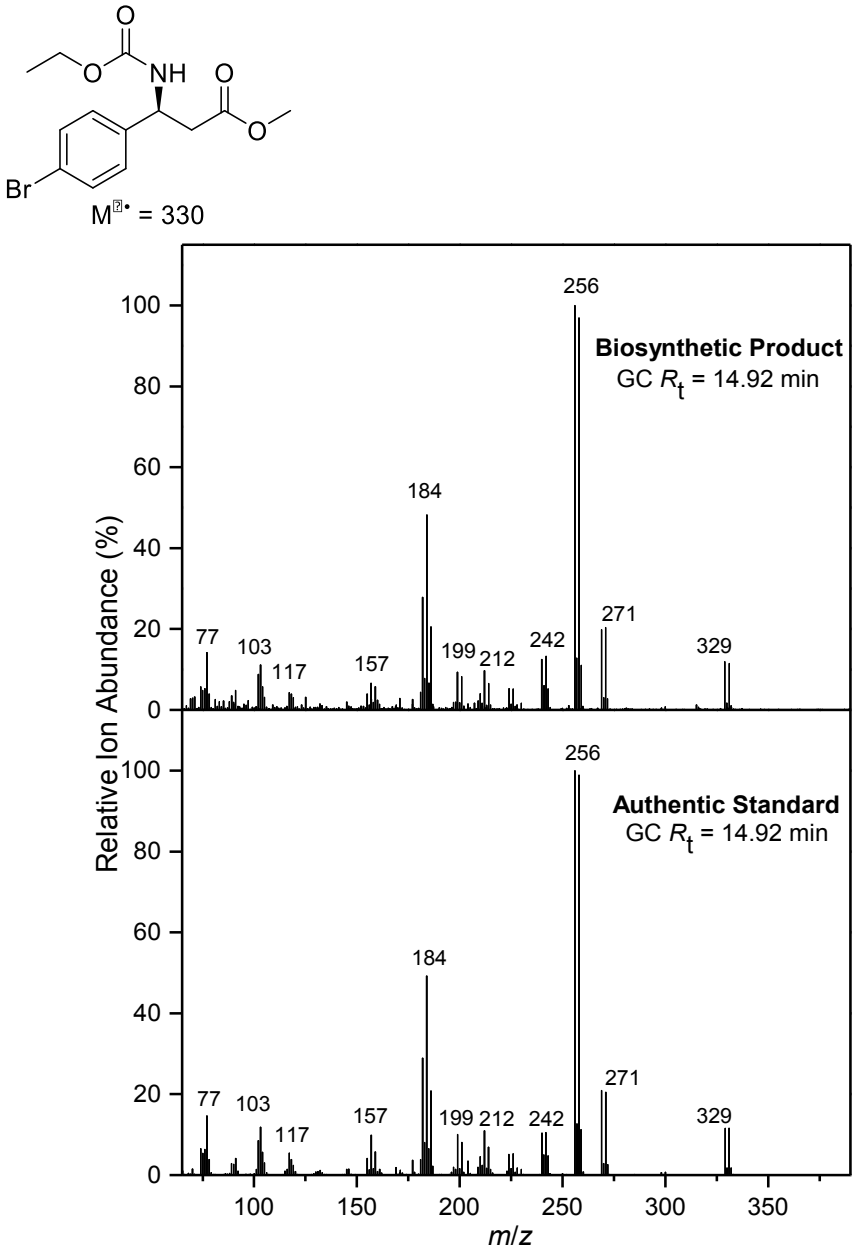

Figure S15. EI-MS spectra of the *N*-(ethoxycarbonyl) methyl ester derivatives of biosynthetic *p*-bromo-β-phenylalanine made from *Pa*PAM catalysis (top) and authentic *p*-bromo-β-phenylalanine (bottom). GC retention times (GC R_t) are shown.

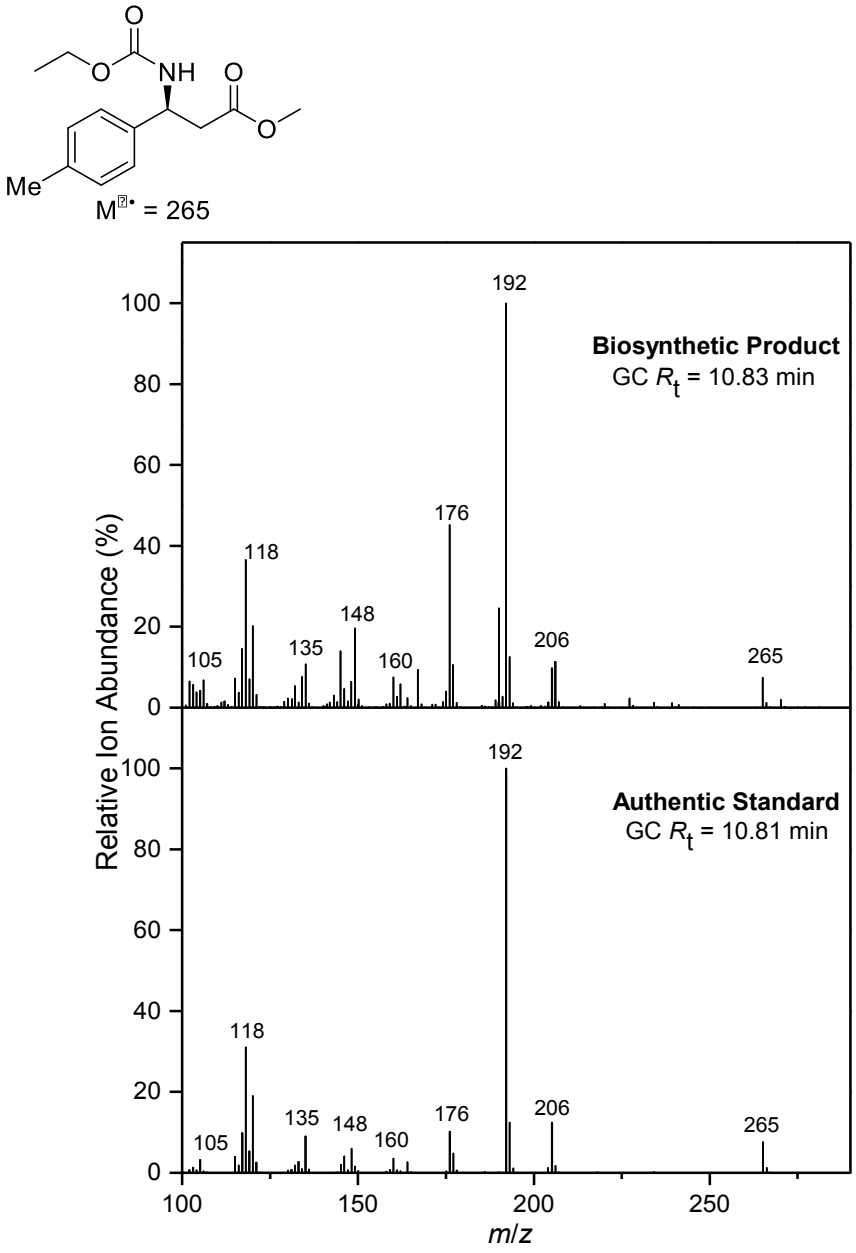

Figure S16. EI-MS spectra of the *N*-(ethoxycarbonyl) methyl ester derivatives of biosynthetic *p*-methyl-β-phenylalanine made from *Pa*PAM catalysis (top) and authentic *p*-methyl-β-phenylalanine (bottom). GC retention times (GC R_t) are shown.

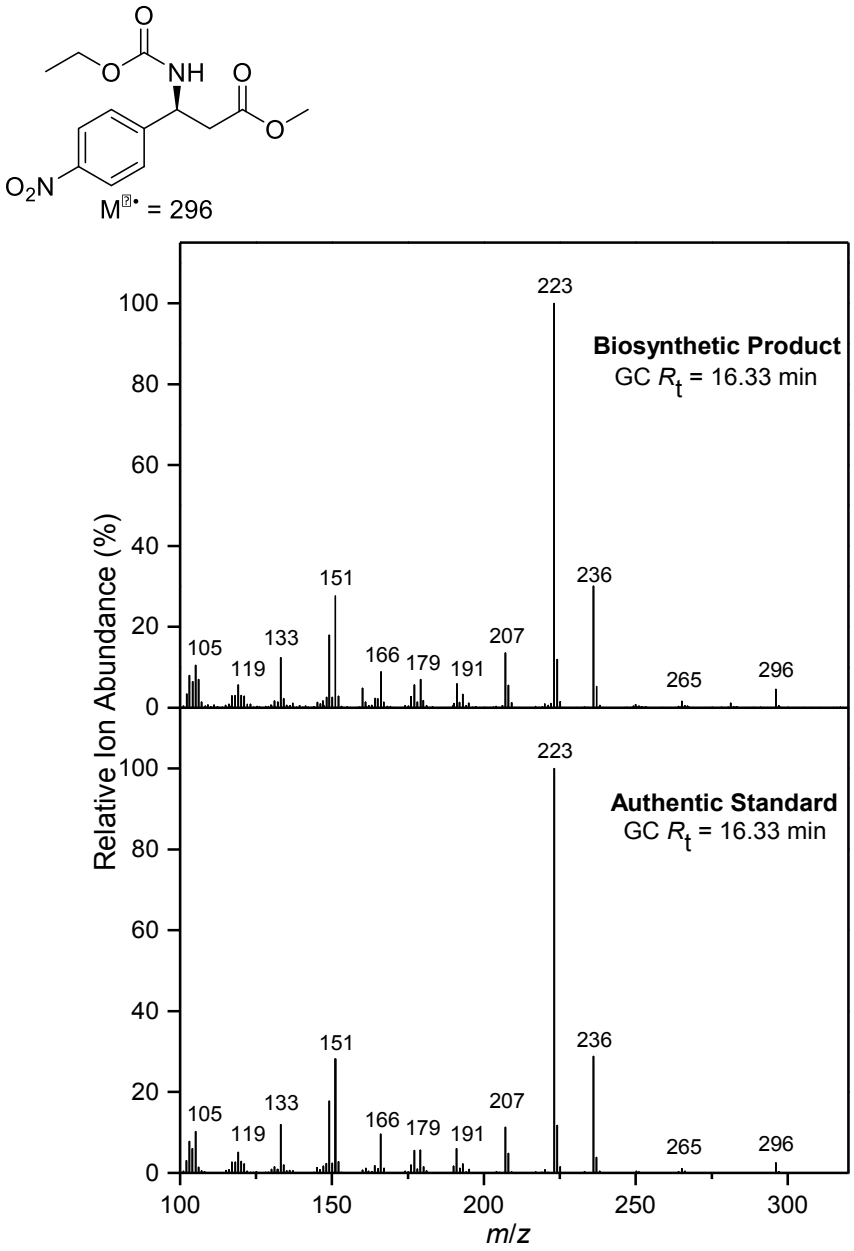

Figure S17. EI-MS spectra of the *N*-(ethoxycarbonyl) methyl ester derivatives of biosynthetic *p*-nitro-β-phenylalanine made from *Pa*PAM catalysis (top) and authentic *p*-nitro-β-phenylalanine (bottom). GC retention times (GC R_t) are shown.

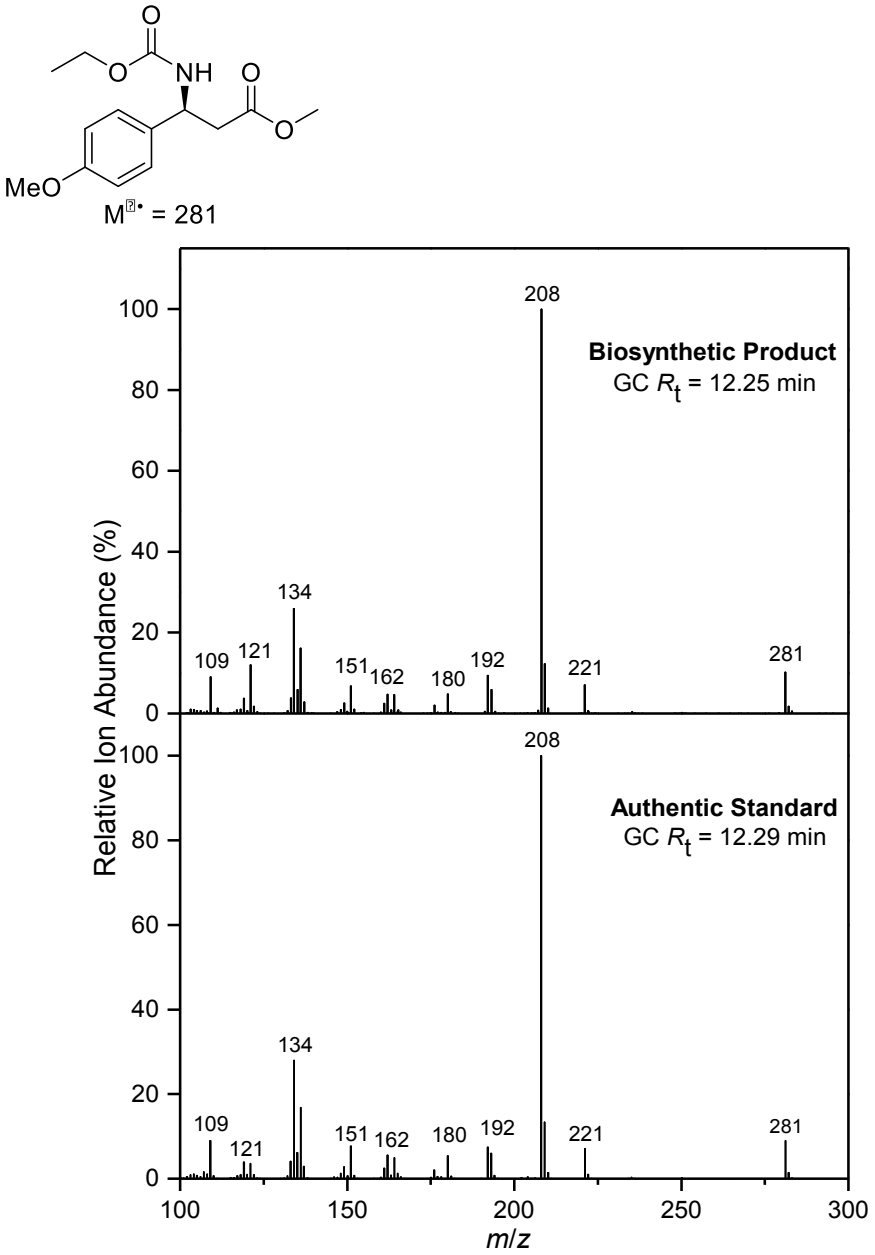

Figure S18. EI-MS spectra of the *N*-(ethoxycarbonyl) methyl ester derivatives of biosynthetic *p*-methoxy-β-phenylalanine made from *Pa*PAM catalysis (top) and authentic *p*-methoxy-β-phenylalanine (bottom). GC retention times (GC R_t) are shown.

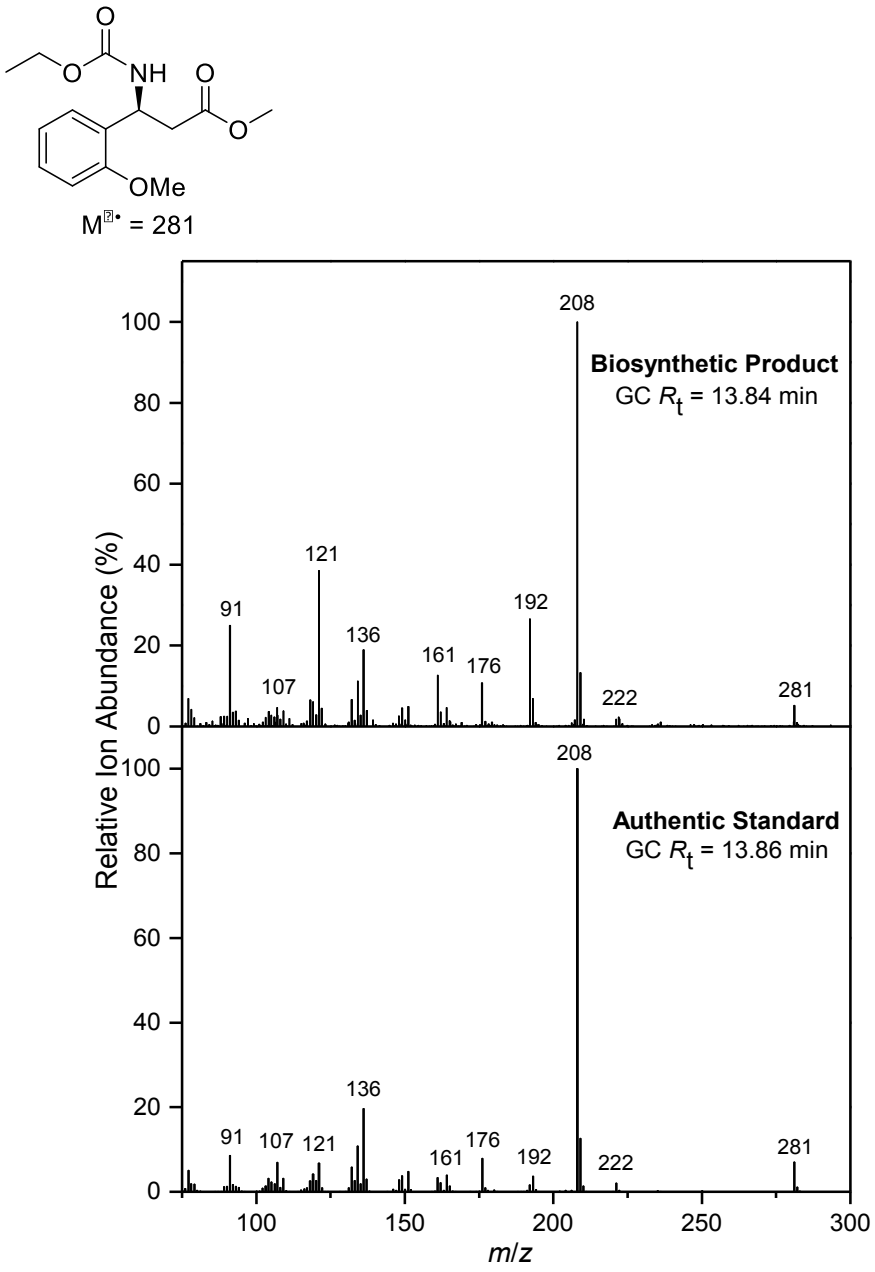

Figure S19. EI-MS spectra of the *N*-(ethoxycarbonyl) methyl ester derivatives of biosynthetic *o*-methoxy-β-phenylalanine made from *Pa*PAM catalysis (top) and authentic *o*-methoxy-β-phenylalanine (bottom). GC retention times (GC R_t) are shown.

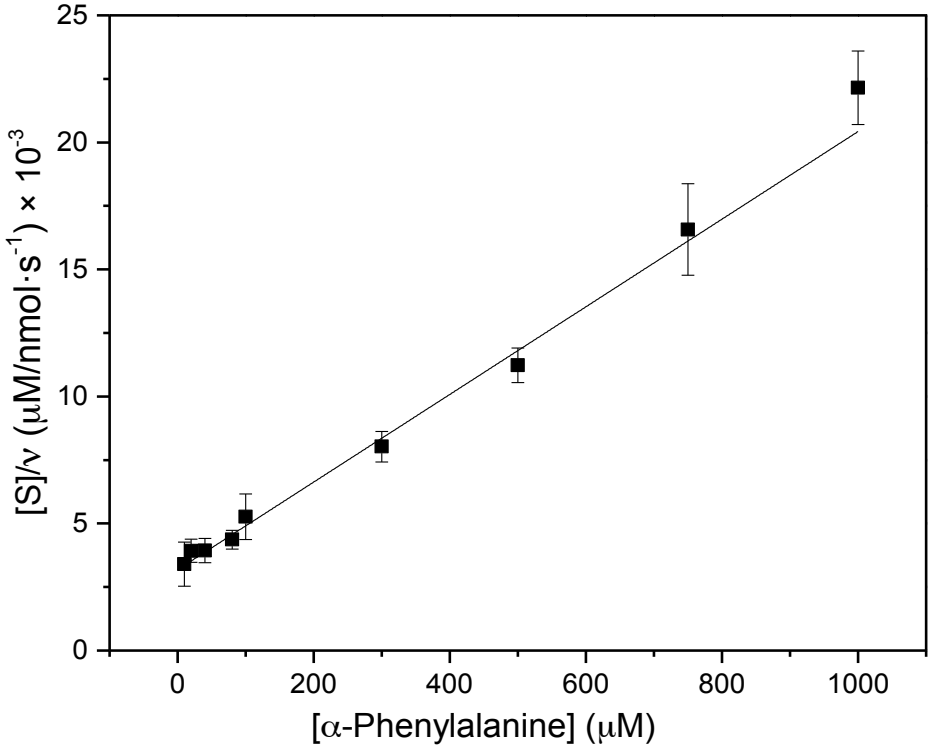

Figure S20. Hanes-Woolf plot of biosynthetic β-phenylalanine (designated as velocity, *v*) catalyzed by *Pa*PAM from α-phenylalanine (S).

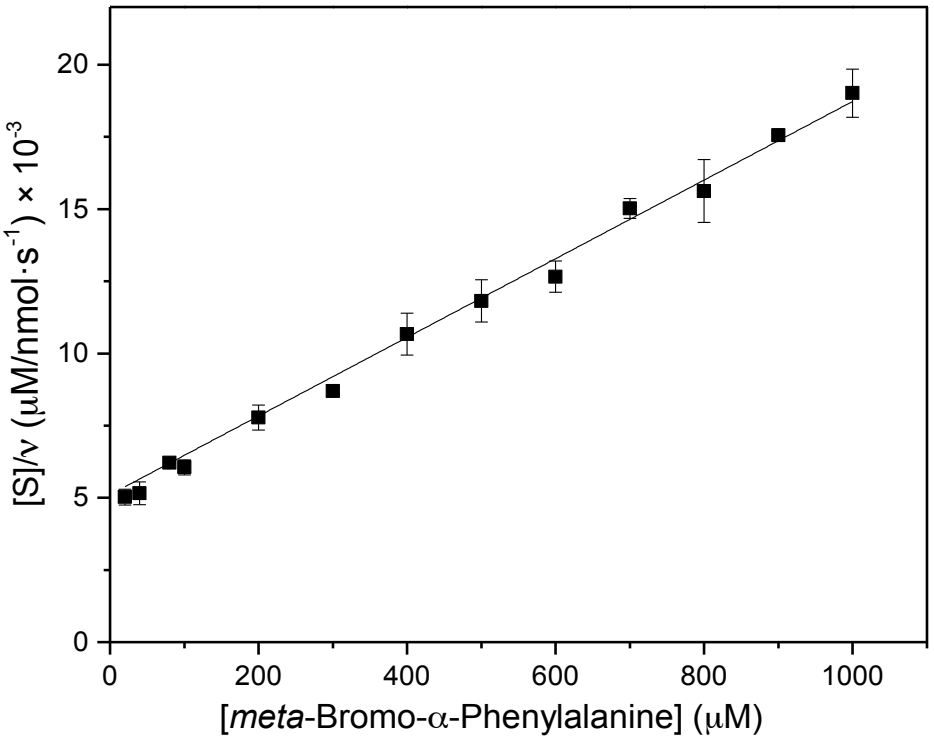

Figure S21. Hanes-Woolf plot of biosynthetic *m*-bromo-β-phenylalanine (designated as velocity, *v*) catalyzed by *Pa*PAM from *m*-bromo-α-phenylalanine (S).

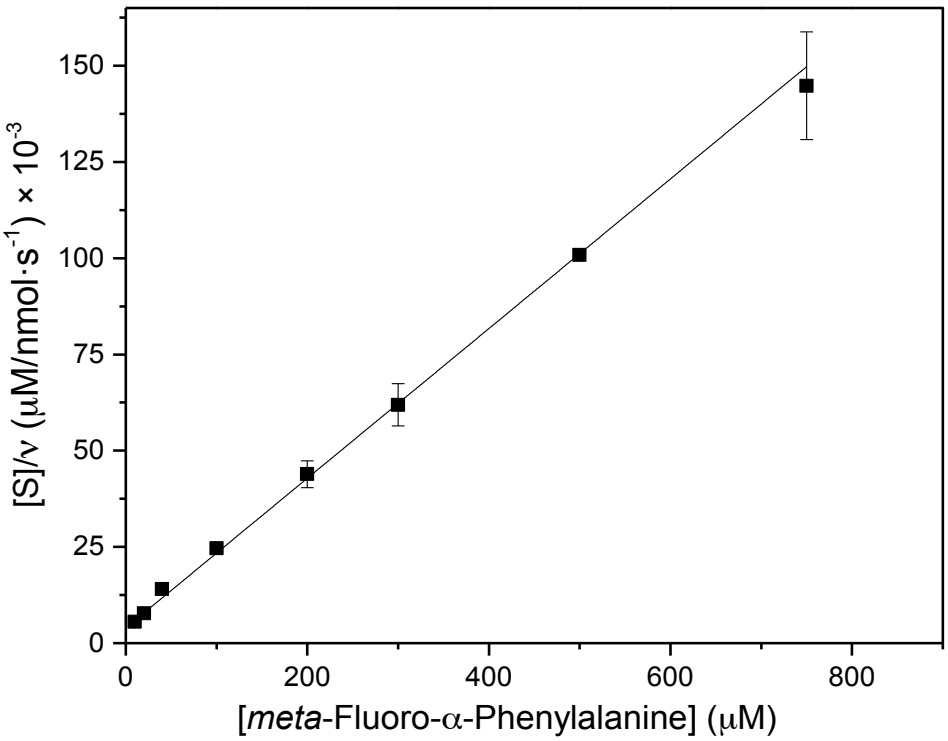

Figure S22. Hanes-Woolf plots of biosynthetic *m*-fluoro-β-phenylalanine (designated as velocity, *v*) catalyzed by *Pa*PAM from *m*-fluoro-α-phenylalanine (S).

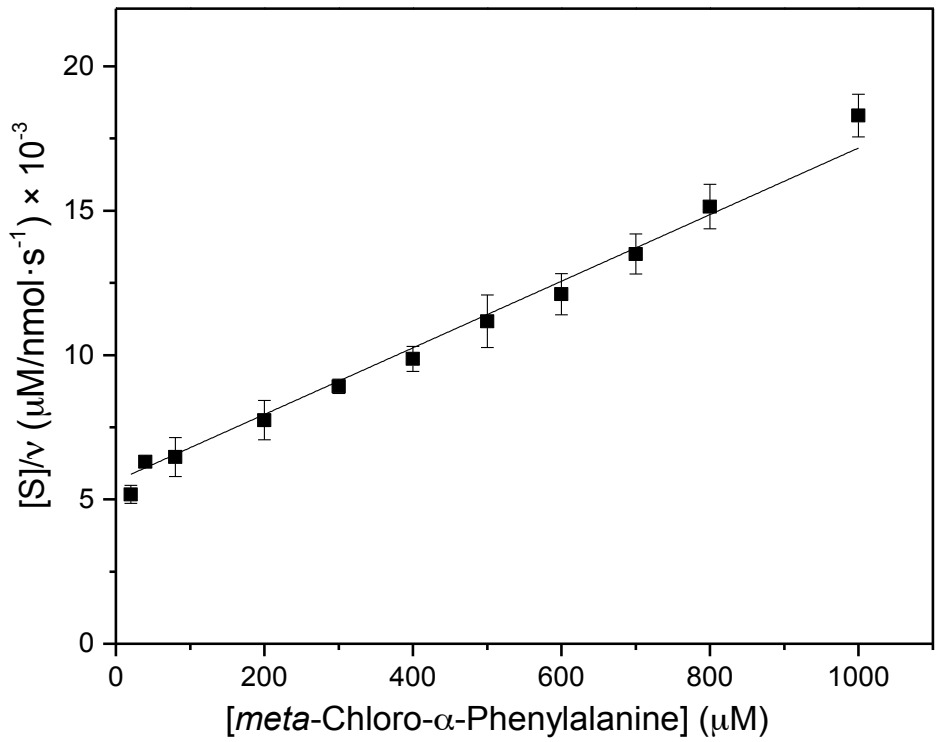

Figure S23. Hanes-Woolf plots of biosynthetic *m*-chloro-β-phenylalanine (designated as velocity, *v*) catalyzed by *Pa*PAM from *m*-chloro-α-phenylalanine (S).

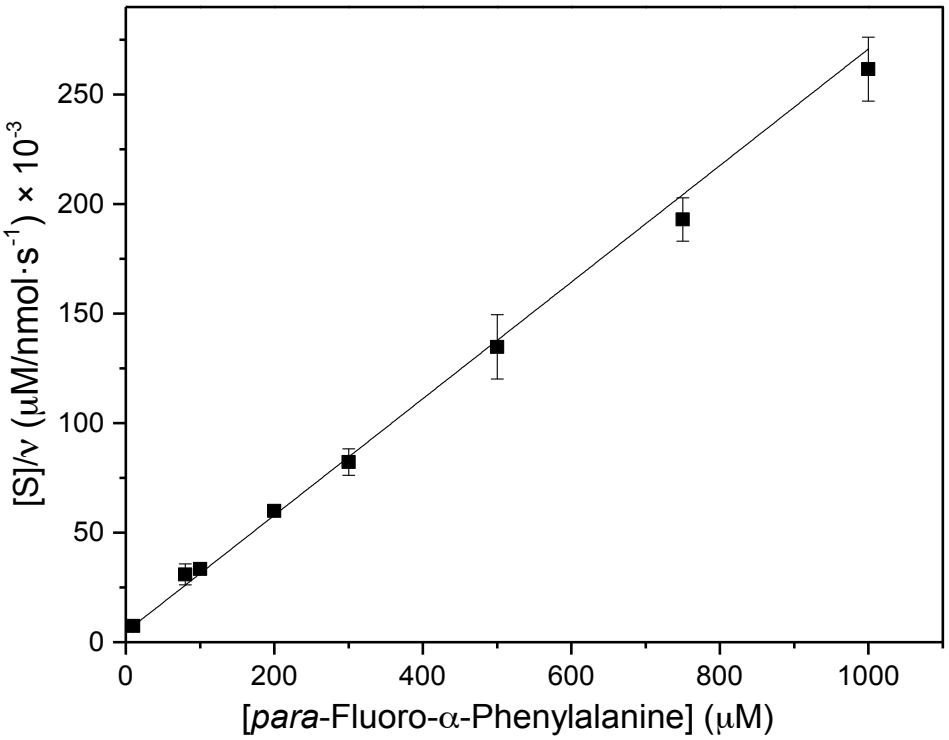

Figure S24. Hanes-Woolf plots of biosynthetic *p*-fluoro-β-phenylalanine (designated as velocity, *v*) catalyzed by *Pa*PAM from *p*-fluoro-α-phenylalanine (S).

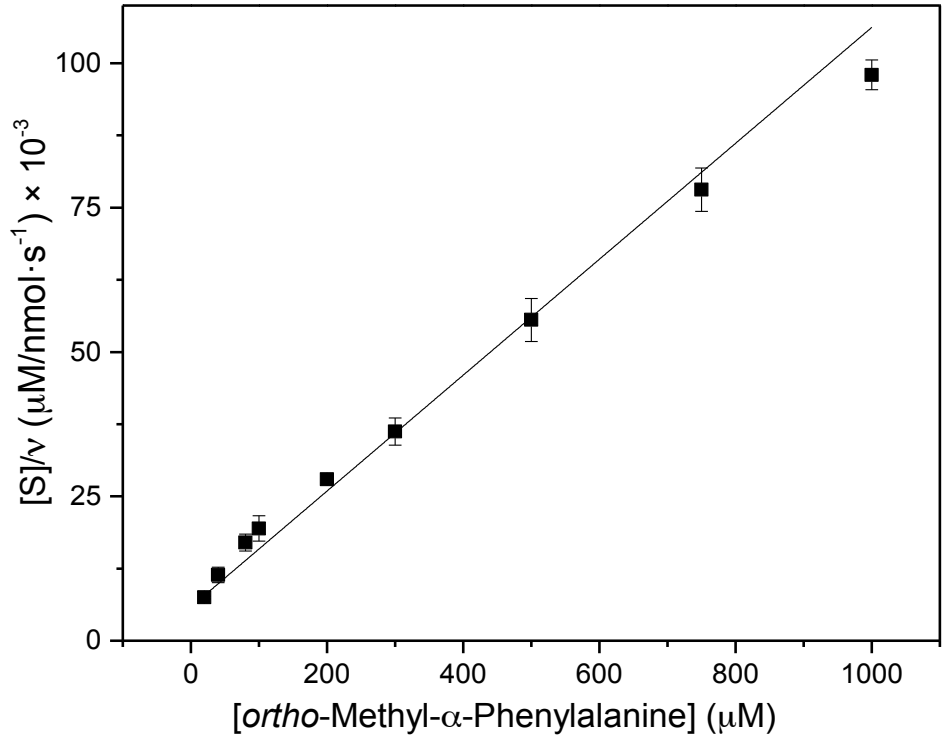

Figure S25. Hanes-Woolf plots of biosynthetic *o*-methyl-β-phenylalanine (designated as velocity, *v*) catalyzed by *Pa*PAM from *o*-methyl-α-phenylalanine (S).

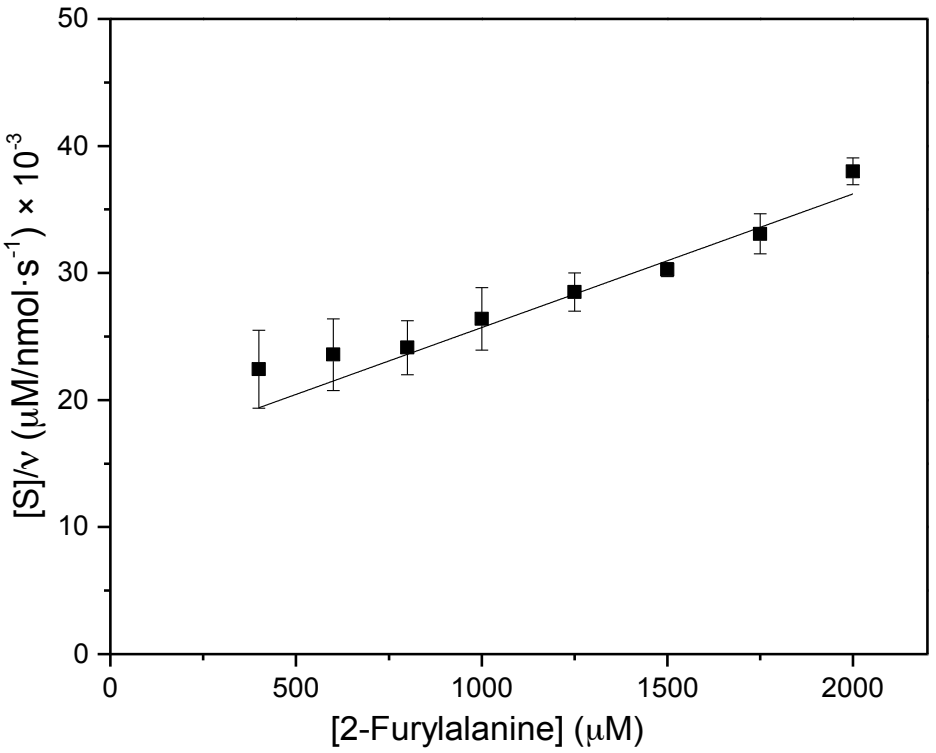

Figure S26. Hanes-Woolf plots of biosynthetic 2-furyl-β-alanine (designated as velocity, *v*) catalyzed by *Pa*PAM from 2-furyl-α-alanine (S).

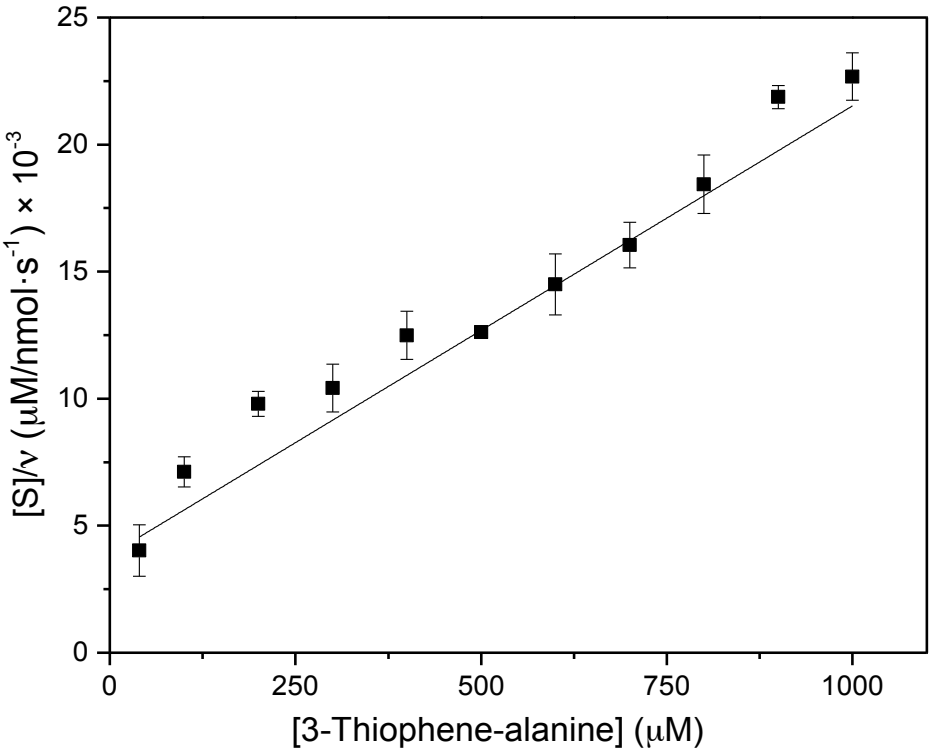

Figure S27. Hanes-Woolf plots of biosynthetic 3-thiophenyl-β-alanine (designated as velocity, *v*) catalyzed by *Pa*PAM from 3-thiophenyl-α-alanine (S).

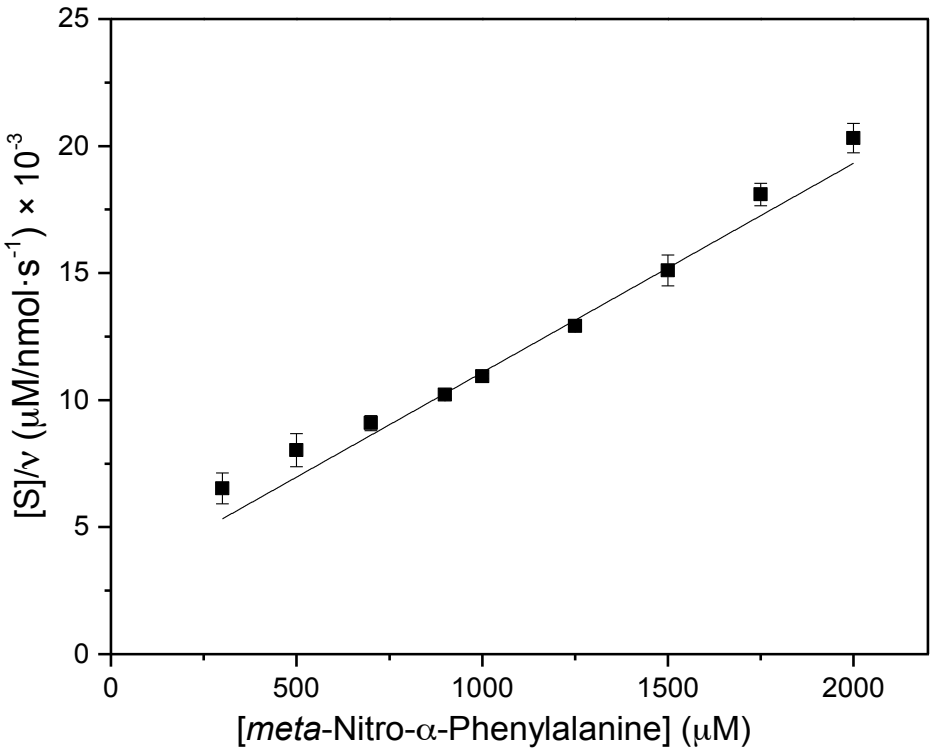

Figure S28. Hanes-Woolf plots of biosynthetic *m*-nitro-β-phenylalanine (designated as velocity, *v*) catalyzed by *Pa*PAM from *m*-nitro-α-phenylalanine (S).

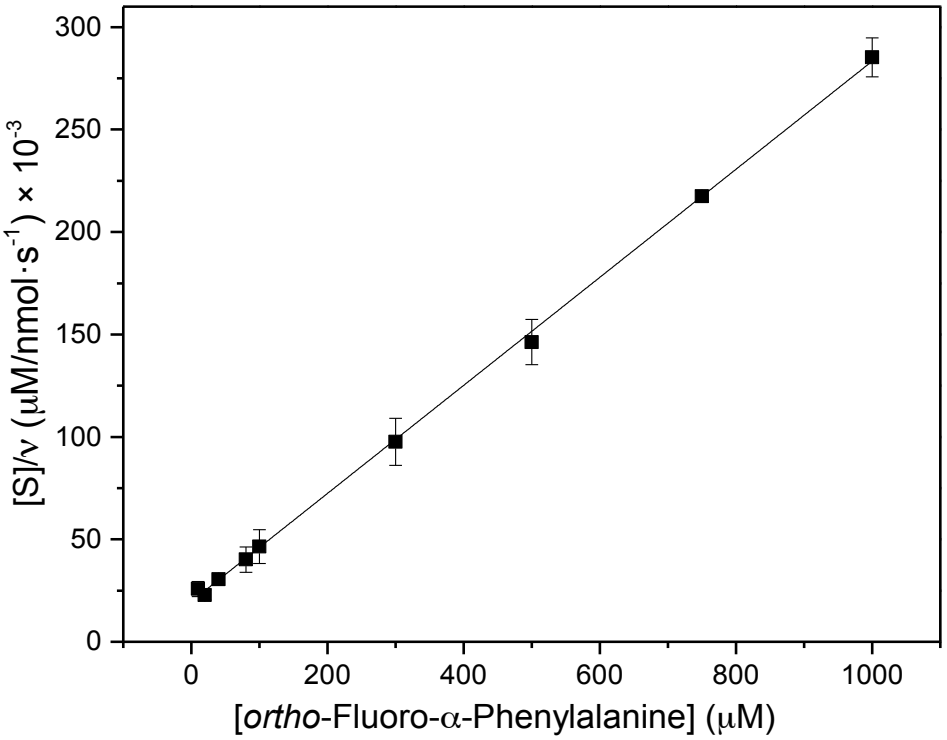

Figure S29. Hanes-Woolf plots of biosynthetic *o*-fluoro-β-phenylalanine (designated as velocity, *v*) catalyzed by *Pa*PAM from *o*-fluoro-α-phenylalanine (S).

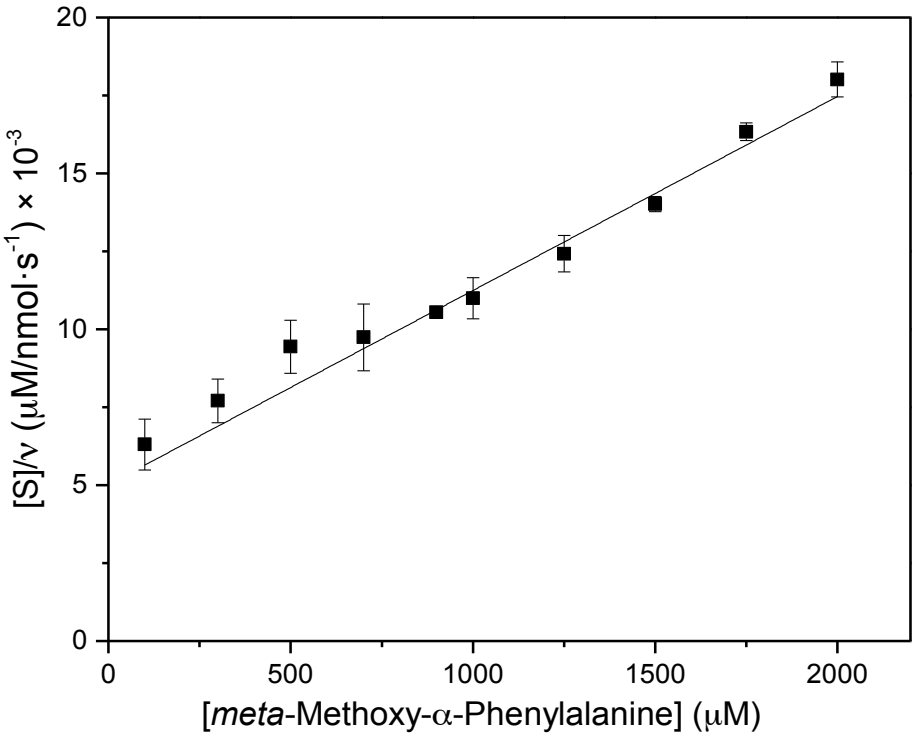

Figure S30. Hanes-Woolf plots of biosynthetic *m*-methoxy-β-phenylalanine (designated as velocity, *v*) catalyzed by *Pa*PAM from *m*-methoxy-α-phenylalanine (S).

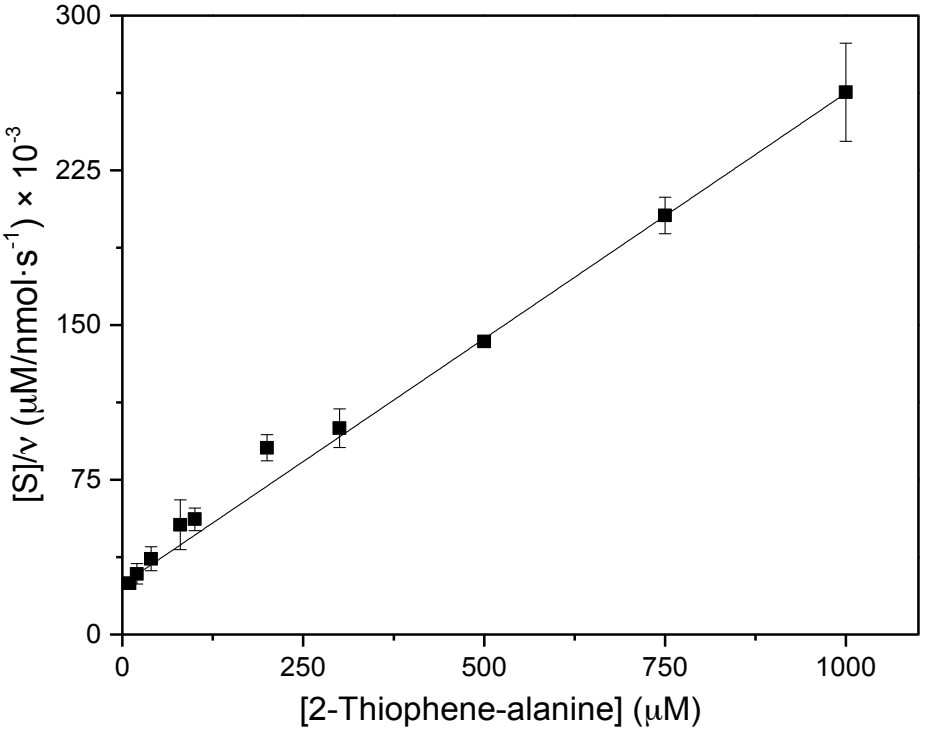

Figure S31. Hanes-Woolf plots of biosynthetic 2-thiophenyl-β-alanine (designated as velocity, *v*) catalyzed by *Pa*PAM from 2-thiophenyl-α-alanine (S).

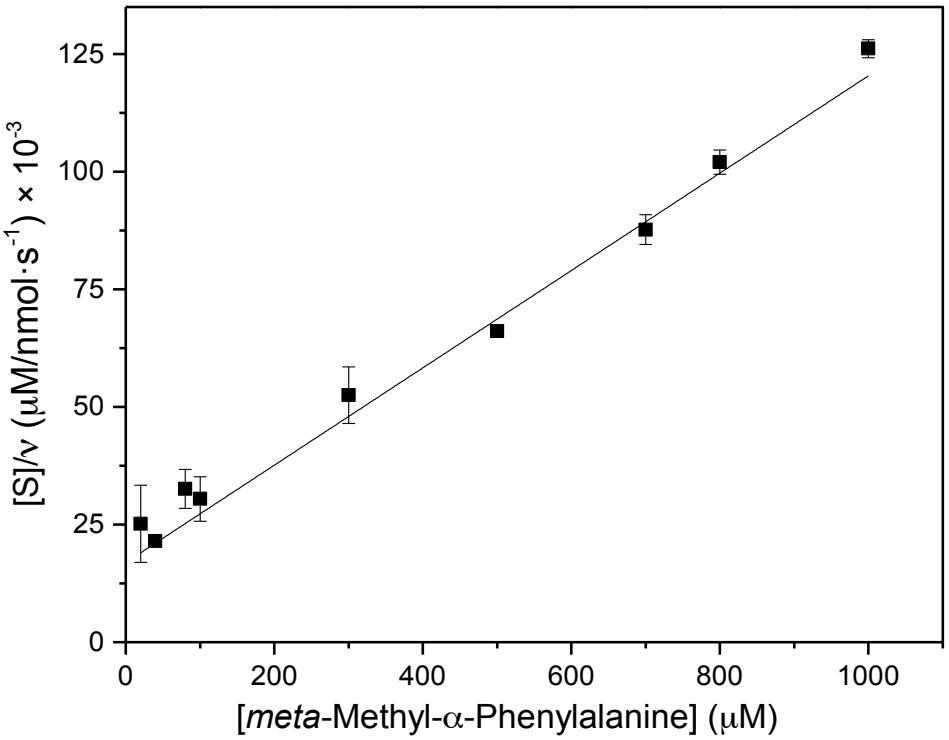

Figure S32. Hanes-Woolf plots of biosynthetic *m*-methyl-β-phenylalanine (designated as velocity, *v*) catalyzed by *Pa*PAM from *m*-methyl-α-phenylalanine (S).

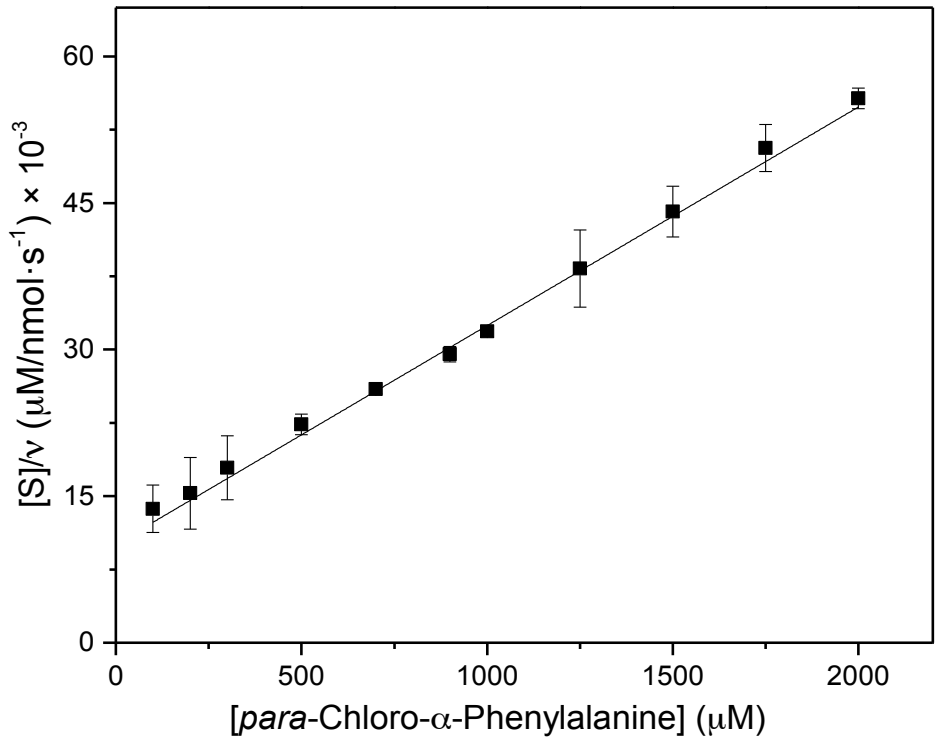

Figure S33. Hanes-Woolf plots of biosynthetic *p*-chloro-β-phenylalanine (designated as velocity, *v*) catalyzed by *Pa*PAM from *p*-chloro-α-phenylalanine (S).

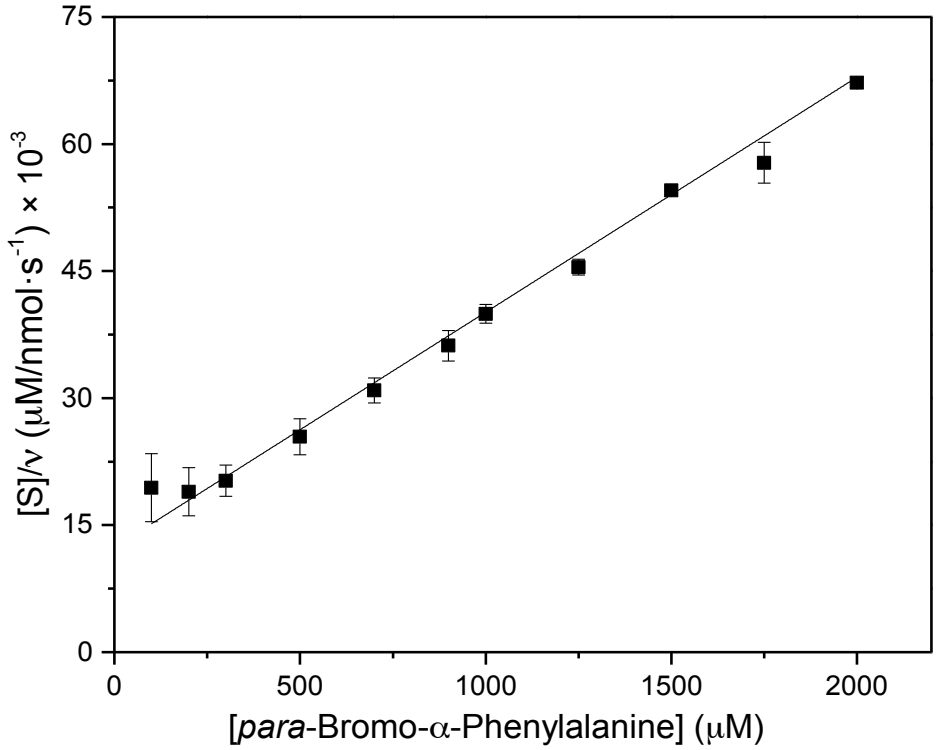

Figure S34. Hanes-Woolf plots of biosynthetic *p*-bromo-β-phenylalanine (designated as velocity, *v*) catalyzed by *Pa*PAM from *p*-bromo-α-phenylalanine (S).

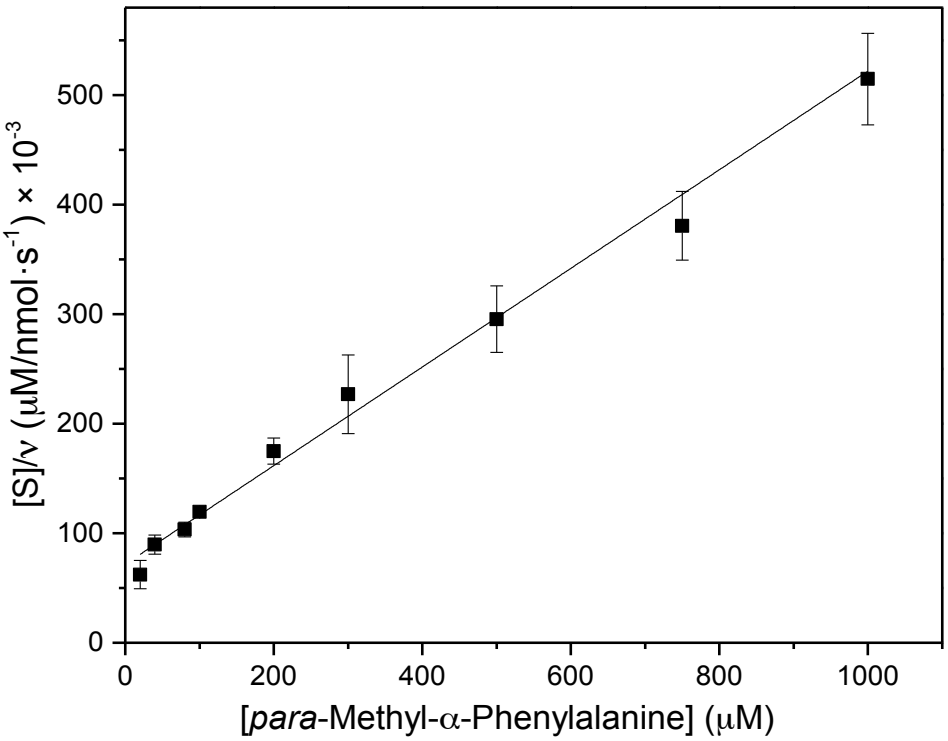

Figure S35. Hanes-Woolf plots of biosynthetic *p*-methyl-β-phenylalanine (designated as velocity, *v*) catalyzed by *Pa*PAM from *p*-methyl-α-phenylalanine (S).

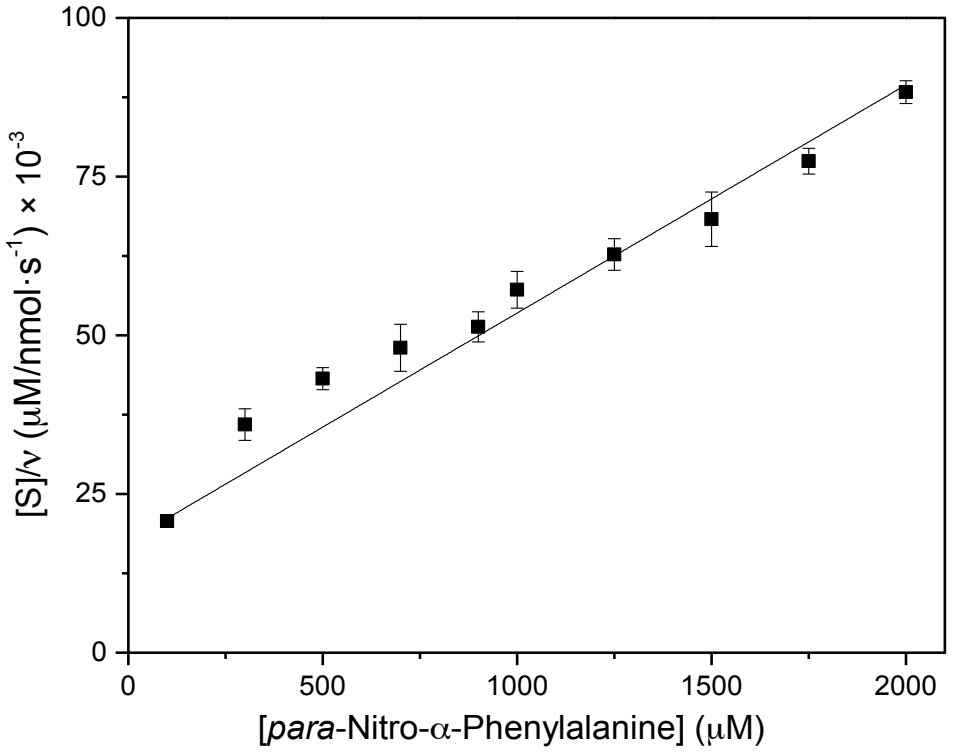

Figure S36. Hanes-Woolf plots of biosynthetic *p*-nitro-β-phenylalanine (designated as velocity, *v*) catalyzed by *Pa*PAM from *p*-nitro-α-phenylalanine (S).

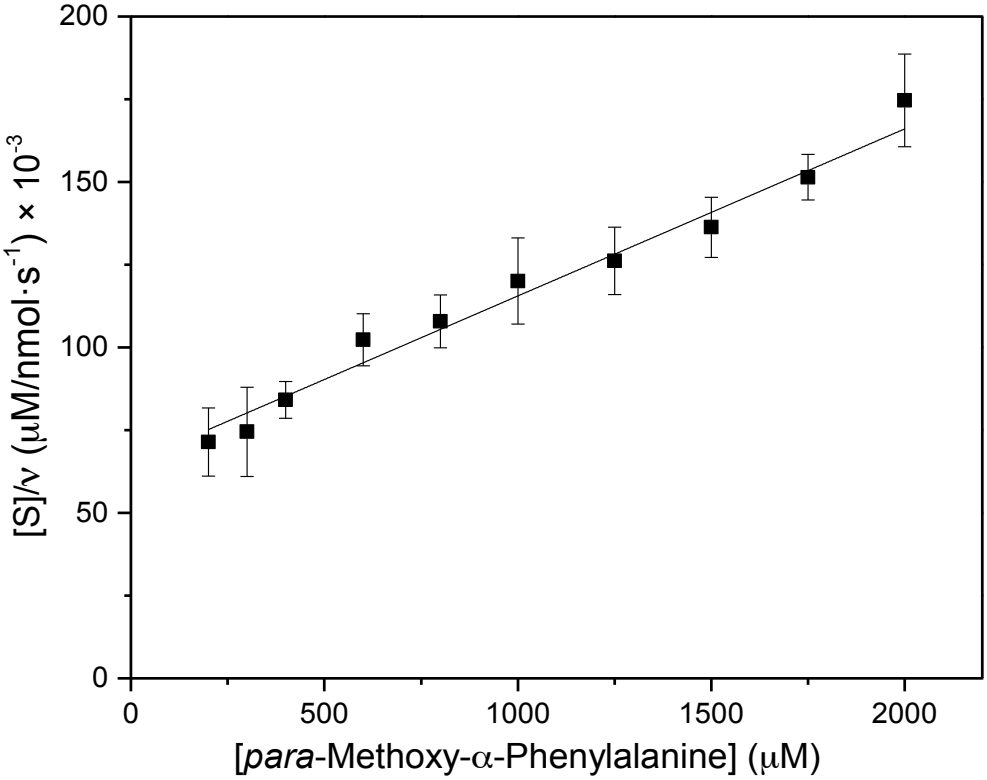

Figure S37. Hanes-Woolf plots of biosynthetic *p*-methoxy-β-phenylalanine (designated as velocity, *v*) catalyzed by *Pa*PAM from *p*-methoxy-α-phenylalanine (S).

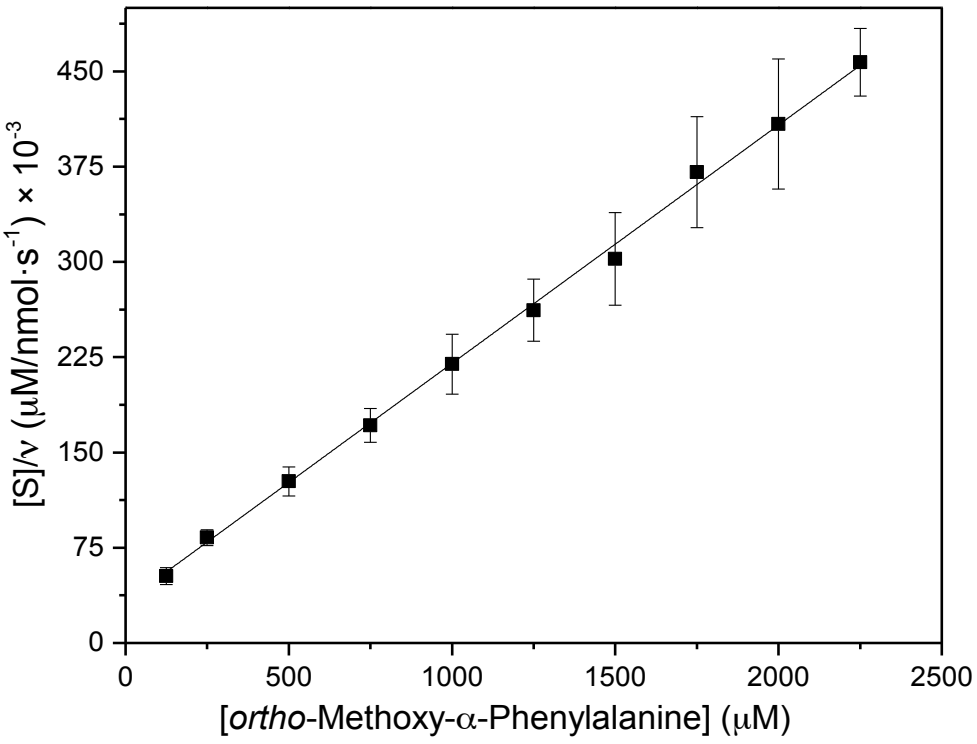

Figure S38. Hanes-Woolf plots of biosynthetic *o*-methoxy-β-phenylalanine (designated as velocity, *v*) catalyzed by *Pa*PAM from *o*-methoxy-α-phenylalanine (S).

Table S1. Comparison of the experimental K_M and predicted energetic order of each substituent at *ortho*-, *meta*-, *para*-positions.

	Fluoro-Substituents[a]			**Chloro-Substituents**[a]			**Bromo-Substituents**[a]		
	***meta*- (3)**	***para*- (5)**	***ortho*- (10)**	***meta*- (4)**	***para*- (14)**	***ortho*- (21)**	***meta*- (2)**	***para*- (15)**	***ortho*- (20)**
K_M (μM)	27	29	73	432	491	-[c]	339	525	-
$E_{V(p-l)}$ (kcal/mol)	19	19	21	33	37	93	55	60	204
$(E_{(p-l)} + E_{(l)})$ (kcal/mol)	148	150	149	166	170	226	188	193	338
	Nitro-Substituents[a]			**Methyl-Substituents**[b]			**Methoxy-Substituents**[b]		
	***meta*- (9)**	***para*- (17)**	***ortho*- (22)**	***ortho*- (6)**	***para*- (16)**	***meta*- (13)**	***ortho*- (19)**	***meta*- (11)**	***para*- (18)**
K_M (μM)	430	752	-	88 (I)	163 (II)	204 (III)	164 (I)	990 (II)	1187 (III)
$E_{V(p-l)}$ (kcal/mol)	48	186	205	55 (III)	46 (II)	40 (I)	108 (III)	86 (II)	81 (I)
$(E_{(p-l)} + E_{(l)})$ (kcal/mol)	236	360	393	190 (III)	179 (II)	174 (I)	292 (III)	240 (II)	219 (I)

[a]Computational approach correctly explained the trends in K_M values of substrate analogs.
[b]Trends in K_M did not correlate well with computationally predicted energy values, which fell within a relatively narrow range. Trends from most (I) to least (III) favorable are shown in (Roman numerals).
[c]Hyphens indicate non-productive substrates.

Table S2. Comparison of the experimental K_M and predicted energetic order of each substituent at *ortho*-, *meta*-, *para*-positions. This data is the same as presented in Table 1S; here, it is organized according to substituent position rather than type.

	***ortho*-Substituents**					
K_M (μM)	**Fluoro**	**Methyl**	**Methoxy**	**Bromo**	**Chloro**	**Nitro**
	73	88	164	-[a]	-	-
$E_{V(p\text{-}l)}$ (kcal/mol)	**Fluoro**	**Methyl**	**Chloro**	**Methoxy**	**Bromo**	**Nitro**
	21	55	93	108	204	205
($E_{(p\text{-}l)}$ + $E_{(l)}$) (kcal/mol)	**Fluoro**	**Methyl**	**Chloro**	**Methoxy**	**Bromo**	**Nitro**
	149	190	226	292	338	393
	***meta*-Substituents**					
K_M (μM)	**Fluoro**	**Methyl**	**Bromo**	**Nitro**	**Chloro**	**Methoxy**
	27	204	339	430	432	990
$E_{V(p\text{-}l)}$ (kcal/mol)	**Fluoro**	**Chloro**	**Methyl**	**Nitro**	**Bromo**	**Methoxy**
	19	33	40	48	55	86
($E_{(p\text{-}l)}$ + $E_{(l)}$) (kcal/mol)	**Fluoro**	**Chloro**	**Methyl**	**Bromo**	**Nitro**	**Methoxy**
	148	166	174	188	236	240
	***para*-Substituents**					
K_M (μM)	**Fluoro**	**Methyl**	**Chloro**	**Bromo**	**Nitro**	**Methoxy**
	29	163	491	525	752	1187
$E_{V(p\text{-}l)}$ (kcal/mol)	**Fluoro**	**Chloro**	**Methyl**	**Bromo**	**Methoxy**	**Nitro**
	19	37	46	60	81	186
($E_{(p\text{-}l)}$ + $E_{(l)}$) (kcal/mol)	**Fluoro**	**Chloro**	**Methyl**	**Bromo**	**Methoxy**	**Nitro**
	150	170	179	193	219	360

[a]Non-productive substrates are indicated by hyphens.

Table S3. Evaluation of protein-ligand and ligand internal energy values and preference for *NH_2-cis* versus *NH_2-trans* configuration**.**

Substrate		***NH_2-trans*** **($E_{(p\text{-}l)} + E_{(l)}$)[a] (kcal/mol)**	***NH_2-cis*** **($E_{(p\text{-}l)} + E_{(l)}$)[a] (kcal/mol)**	**$E_{V(p\text{-}l)}$[b] (kcal/mol)**	**K_M (μM)**	**Preferred Orientation[c]**
1	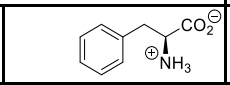	149	149	19	168	Symmetrical[d]
2	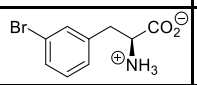	429	188	55	339	*NH_2-cis*
3	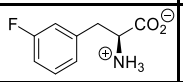	153	148	19	27	NSD[e]
4	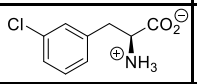	273	166	33	432	*NH_2-cis*
5	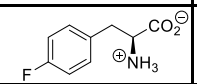	150	150	19	29	Symmetrical
6	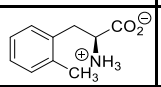	190	489	55	88	*NH_2-trans*
7	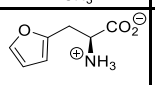	133	115	21	415	NSD
8	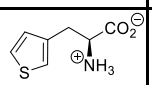	156	154	21	337	NSD
9	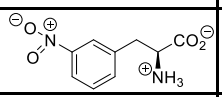	1640	236	48	430	*NH_2-cis*
10	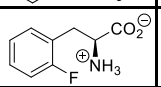	149	165	21	73	NSD
11	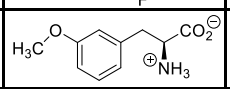	265	240	86	990	NSD
12	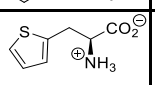	132	139	20	132	NSD
13	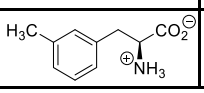	245	174	40	204	*NH_2-cis*

Table S3S continued on next page

14	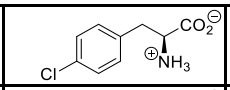	170	170	37	491	Symmetrical
15	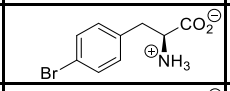	193	193	60	525	Symmetrical
16	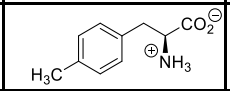	179	179	46	163	Symmetrical
17	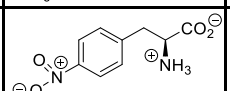	360	360	186	752	Symmetrical
18	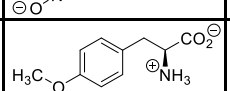	219	947	81	1187	*NH_2-trans*
19	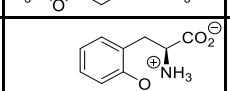	409	292	108	164	*NH_2-cis*
20	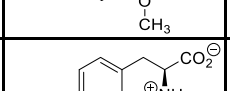	338	525	204	-[f]	*NH_2-trans*
21	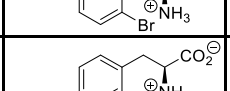	226	401	93	-	*NH_2-trans*
22	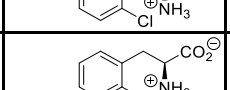	393	2065	205	-	*NH_2-trans*

[a]($E_{(p\text{-}l)}$ + $E_{(l)}$) is the sum of protein-ligand and ligand internal energy, where $E_{(p\text{-}l)}$ is the protein-ligand interaction energy and $E_{(l)}$ is the ligand internal energy. [b]$E_{\boldsymbol{V(p\text{-}l)}}$ is the vdW energy of protein-ligand interaction, one of the terms contributing to $E_{(p\text{-}l)}$. The vdW energy is given for whichever orientation (*NH_2-cis* or *NH_2-trans*) had the lower, more favorable ($E_{(p\text{-}l)}$ + $E_{(l)}$) value. [c]Substrates were categorized as preferring an *NH_2-cis* or *NH_2-trans* configuration if the given orientation was at least 25 kcal/mol lower in ($E_{(p\text{-}l)}$ + $E_{(l)}$) value. [d]α-Phenylalanine and *para*-substituted substrates have symmetrical aryl rings with equal interaction energies for the *NH_2-cis* and *NH_2-trans* configurations. [e]Substrates observed to have no significant difference (NSD) in energy for the *NH_2-cis* or *NH_2-trans* configuration. [f]Non-productive substrates are indicated by hyphens. Note, all energies reported should be considered relative rather than absolute.

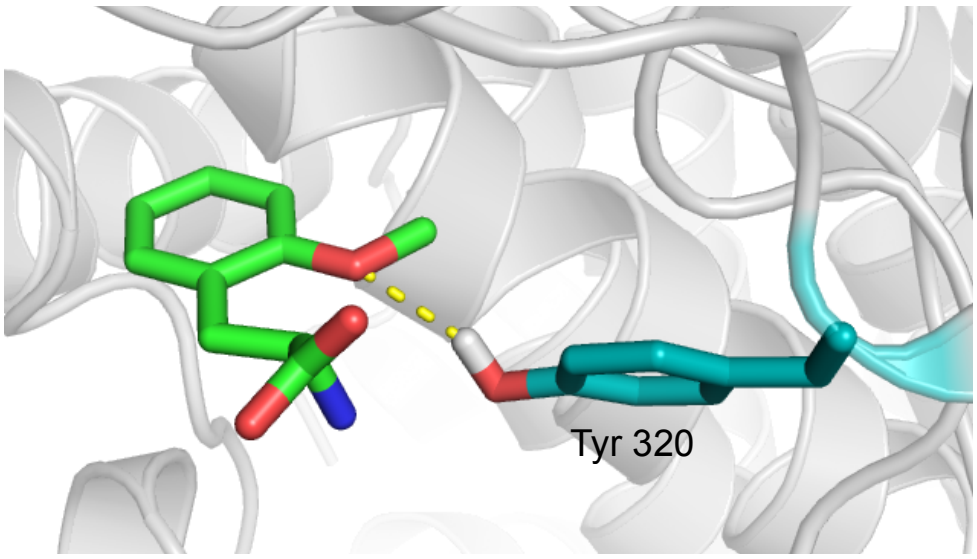

Figure S39. H-bonding interaction of *ortho*-methoxy-α-phenylalanine (**19**) and active site Tyr320. *o*-Methoxy-α-phenylalanine atoms are colored as C, green; N, blue; O, red and Tyr320 atoms are colored as C, light blue; O, red; H, white.

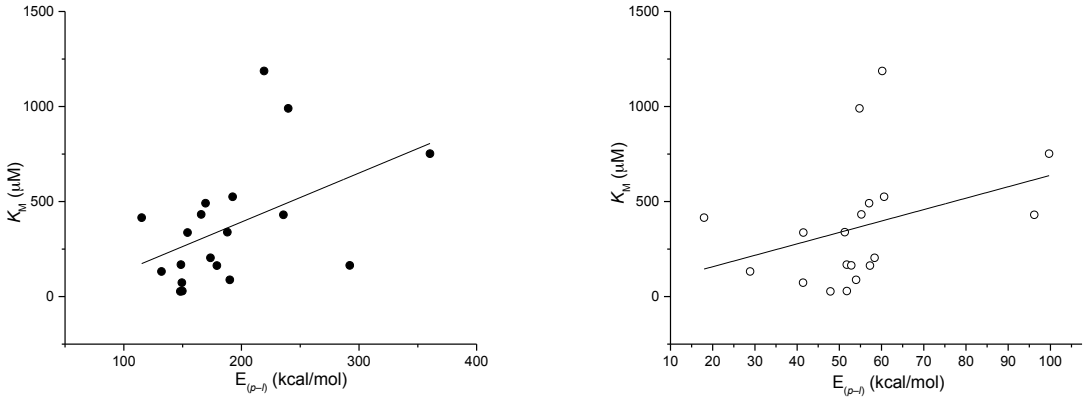

Figure S40. Relationship between protein-ligand interaction energy $E_{(p\text{-}l)}$ and experimental K_M. Substrates were placed in the active site in *NH_2-cis* and *NH_2-trans* orientations overlaid with the crystallographic orientation of α-phenylalanine from PDB entry 3UNV, and the lower energy orientation was kept. Left panel: (●) Binding site residues of *Pa*PAM were maintained in their crystallographic orientation, yielding a linear correlation coefficient of 0.48 between $E_{(p\text{-}l)}$ and experimental K_M. Right panel: (○) Energy minimization was used to reduce any repulsive interactions, leading to lower correlation between the resulting protein-ligand interaction energy and K_M value (correlation coefficient = 0.35).

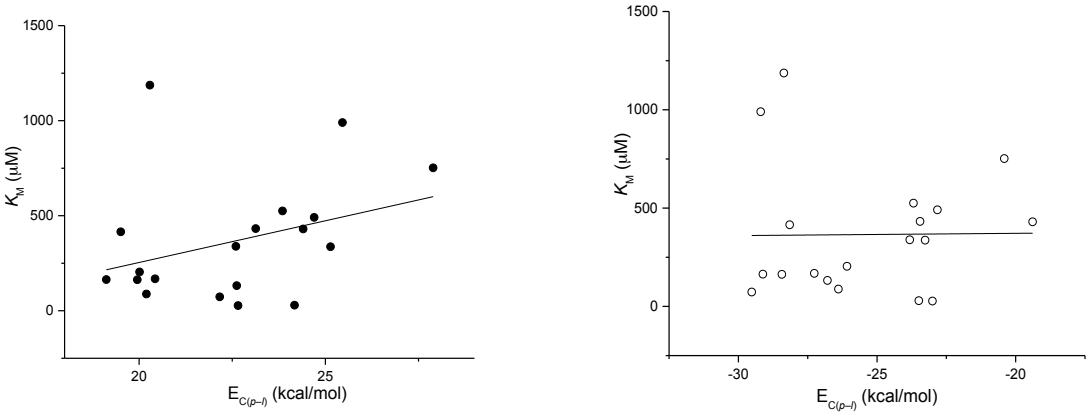

Figure S41. Relationship between the electrostatic (Coulombic) component of the protein-ligand interaction energy $E_{C(p\text{-}l)}$ and experimental K_M. Substrates were placed in the active site in *NH_2-cis* and *NH_2-trans* configurations overlaid with the crystallographic orientation of α-phenylalanine, and the lower energy orientation was kept. Left panel: (●) Binding site of *Pa*PAM was kept in the crystallographic orientation (correlation coefficient = 0.33). Right panel: (○) Energy minimization was used to reduce any protein-ligand repulsive interactions (correlation coefficient = 0.011).

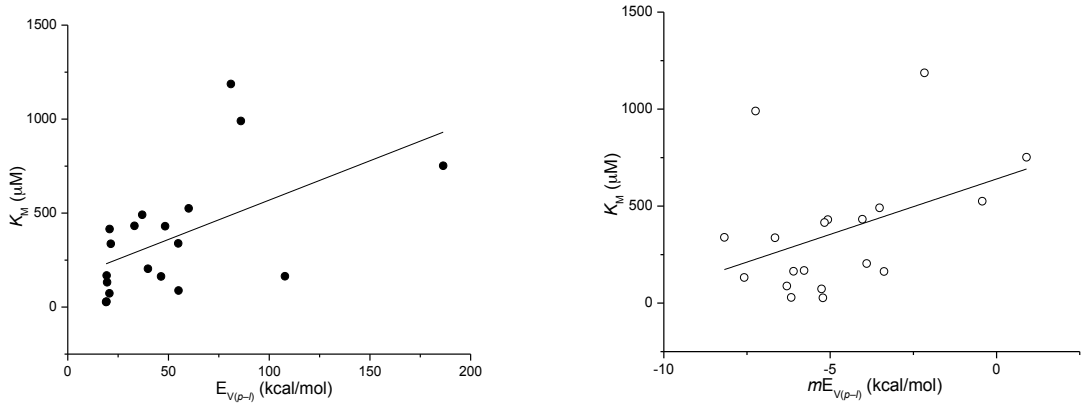

Figure S42. Relationship between the van der Waals energy component of the protein-ligand energy $E_{V(p\text{-}l)}$ and experimental K_M. Substrates were again placed in *NH_2-cis* and *NH_2-trans* orientations overlaid with the crystallographic orientation of α-phenylalanine from PDB entry 3UNV, and the lower energy orientation was kept. Left panel: (●) Binding site residues of *Pa*PAM were kept in the crystallographic orientation (correlation coefficient = 0.54). Right panel: (○) Energy minimization was used to reduce any protein-ligand repulsive interactions (correlation coefficient = 0.42). These results indicate that the van der Waals interaction energy between the protein and each substrate overlaid with the α-phenylalanine-bound crystal structure is most predictive of the relative K_M values of the substrates.